KASPARS MICULIS

Stochastic Dynamics, Ionisation, and Radiative Energy Transfer in Optically Excited Alkali Gases

Résumé of promotion work

University of Latvia

Riga - 2006

Abstract

A subject of this thesis work is the excitation energy transfer and ionization processes in optically excited alkali gases. In this work ionization processes and radiative resonance energy transfer in atomic vapours are theoretically investigated. Several theoretical methods are developed in order to describe complicated atom-atom collision processes, photoionization, photodissociation and associative ionization processes in excited alkali gases.

In atomic vapours when atoms are colliding usually a short-lived quasi-molecular system is produced. For exact quantum chemical approaches to the analysis of this quasi-molecular system already a precise calculation of a single potential surface of a system as simple as triatomic is a challenge, not to talk about processes in which several potential surfaces are involved. Such calculations require complicated computational procedures, which are extremely demanding in terms of computer resources and susceptible to errors. Therefore the chances to achieve reliable results using only the exact quantum chemical approaches are questionable. This is especially true when one of the partners of the atomic encounter is in a highly excited state, or when the collision complex appears in a highly excited state during the encounter. Under such conditions one has to deal with multiple surface crossings and overlapping dynamic resonances. They induce chaos-like instabilities in the evolution of trajectories of weakly bound electrons or atoms, eventually leading to ionisation or fragmentation. Such chaotic processes can be described by the stochastic theory. **One of the tasks of this thesis is theoretical description of the stochastic phenomena in atomic collisions and assessment of the applicability of the kinetic Fokker-Planck-like diffusion equations for the description of the evolution of collision complexes within a dense spectrum of energy states.** The obtained results demonstrate the complexity of ionization processes following excitation of atomic Rydberg states, and indicate the path along which ionization of more complex systems involving molecules can be studied both experimentally and theoretically. The stochastic theory was developed in collaboration with prof. N. Bezuglov from St. Petersburg State University, Russia. It treats the ionization as excitation of Rydberg electrons to the continuum by the electric dipole field generated by exchange interaction within the quasi-molecular ion.

In the stochastic theory, redistribution of the population prior to ionization over a range of Rydberg states due to non-adiabatic processes in overlapping multiple level crossings of quasi-molecular Rydberg states is described in terms of stochastic diffusion of electrons. This diffusion process in the Rydberg energy spectrum is analyzed using a Fokker-Planck type equation. In this work we are making the first attempt to take into account the stochastic motion of Rydberg electron and apply this model to describe several atomic collision processes. Collisions leading to the formation of atomic (*Penning ionization* - PI) or molecular ions (*associative ionization* - AI) have been studied. The stochastic processes are expected to become increasingly important in low temperature systems with reduced collision velocities and increased collision times, like an ensemble of ultracold atoms in a magneto-optical trap (MOT). Other important motivation to develop stochastic theory is the quest for active control of chemical processes.

The second problem addressed in this thesis work is related to photoionization and photo transition processes in sodium atom. This part of thesis deals with obtaining atomic data that are needed for various scientific studies. Of particular interest was the prediction of radiative lifetimes of excited atomic energy states. Ocscillator strengths and transition probabilities to discrete atomic levels and to continuum states are often needed in contemporary atomic physics experiments. This was the main motivation of this part of the thesis work. Studies of literature showed that the existing transition probability data of alkali atoms is limited to relatively low excited states, whereas for Rydberg states they were usually extracted by using in part oversimplified estimates. **The second task of the present work was to calculate phototransition probabilities of Na($3p_{3/2}$) atoms to the high Rydberg states and to the ionization continuum.** To achieve this task we used the model potential method, which has been already successfully exploited by other authors in seventies and eighties of the last century. The parameters of the potentials used in our work were adjusted to reproduce the experimental energy eigenvalues. The effects of further small interaction terms on the valence electron were also taken into account.

The third task of the thesis work is the investigation of the radiation trapping in optically excited gases in complicated gas cell geometries and calculation of radiation trapping factors in elliptical gas cells. For this purpose we construct analytical solution of Biberman-Holstein radiation trapping equation using a new

semiclassical approach for multi-dimensional semiclassical quantization laws called geometrical quantization technique (GQT). If the absorbing medium is sufficiently optically thick, the radiation in it will undergo several reabsorption and reemission events before escaping from the medium. Radiation trapping in an atomic vapour can influence many spectroscopic experiments. For example, radiation trapping plays an important role in photodissociation experiment in supersonic Na/Na_2 beam analyzed in this thesis. Radiation trapping influences alo velocity distribution of photodissociation fragments and because of that also the rate constants of the reactions. In 1947 Holstein and Biberman independently proposed a Boltzmann-type integro-differential equation describing this phenomenon, and this equation remains the starting point of most of the radiation trapping models. In our study we interpret the basic integro-differential trapping equation as a generalized wave equation for an associated hypothetical quasiparticle. Some modifications of the multi-dimensional semiclassical quantization laws (GQT) allowed us to determine analytically the trapping factors for all practically occurring line-shapes, all opacities, and all modes in a large variety of practically important types of 1D, 2D and 3D vapour cell geometries, for which the separation of spatial variables is possible. An important point is that there are no geometrical (and topological) differences between GQT for the Biberman-Holstein trapping equation and conventional semiclassical billiard-like theories because of the similarity in the trajectories (straight lines within the cell, connecting reflection points on the walls).

The next – fourth – task of the promotion work is related to the investigation of a photodissociation of sodium molecules $Na_2(X^1\Sigma_g^+, v'')$ in supersonic Na/Na_2 beam and calculations of cross sections for photodissociation of sodium molecules $Na_2(X^1\Sigma_g^+, v'')$ by λ_{PD} = 458 nm radiation from an Ar^+ ion laser, required for the interpretation of an imaging experiment with this photodissociation process. It was assumed that the electronic wavefunction can instantaneously adjust as the molecular bonds stretch, break, and finally form the free toms. This implicit assumption known as the electronically adiabatic or the Born-Oppenheimer approximation was used by us in a simple two-state model. Exact knowledge of the photodissociation cross sections allows calibration and testing of experimental set-up. Such testing method can be used also for other spectroscopic experiments.

Results are presented in the publications [publ1-publ7] constituting the thesis:

[publ1] N.N.Bezuglov, V.M.Borodin, V.Grushevskyi, A.N.Klyucharev, **K.Michulis**, F.Fuso and M.Allegrini, *Diffusion ionization of the Rydberg diatomic quasimolecular complex formed upon collisions of rubidium atoms*, Opt. Spectrosc. **95**, 515-524 (2003)

[publ2] I. I. Ryabtsev, D. B. Tretyakov, I. I. Beterov, N. N. Bezuglov, **K. Miculis**, and A. Ekers, *Collisional and thermal ionization of sodium Rydberg atoms I. Experiment for n S and nD atoms with n =8-20*, J. Phys. B **38**, S17-S35 (2005).

[publ3] **K. Miculis**, N. N. Bezuglov, I. I. Beterov, I. I. Ryabtsev, D. B. Tretyakov, A. Ekers, and A. N. Klucharev, *Collisional and thermal ionization of sodium Rydberg atoms II. Theory for n S, nP, and nD states with n = 5-25*, J. Phys. B **38**, 1811-1831 (2005)

[publ4] I.I.Beterov, D.B.Tretyakov, I.I.Ryabtsev, N.N.Bezuglov, **K.Miculis**, A.Ekers, A.N.Klucharev , *Collisional and thermal ionization of sodium Rydberg atoms III. Experiment and theory for nS and nD states with n=8-20 in a crossed beam geometry,* J. Phys. B **38**, 4349-4361 (2005)

[publ5] **K. Miculis**, W. Meyer, *Phototransition of Na($3p_{3/2}$) into high Rydberg states and the ionization continuum,* J. Phys. B **38**, 2097-2108 (2005)

[publ6] N. N. Bezuglov, A. K. Kazanskii, A. N. Klyucharev, **K. Michulis**, F. Fuzo, M. Allegrini, *On accounting for the effect of particles of a condensed dispersed phase on radiant energy transfer in gaseous media,* Opt. Spectrosc. **95**, 631-637 (2003)

[publ7] O. Kaufmann, A. Ekers, K. Bergmann, N. Bezuglov, **K. Miculis**, M. Auzinsh, and W. Meyer, *Velocity redistribution of excited atoms by radiative excitation transfer I. Experimental demonstration by photodissociation of Na_2 and field-free imaging*, J. Chem. Phys. **119,** 3174-3186 (2003)

CONTENTS

Introduction

The alkali metal vapour plays an important role in the modern spectroscopy as a test media for new experimental methods and theoretical approaches. At the same time an alkali atom vapour serves also as a media which allows to implement advanced technological solutions. For example, the most sensitive magnetometers currently are using rubidium vapour as a main ingredient.

When an interaction of alkali vapours with laser radiation is analyzed, one can not neglect ionization processes, radiation transfer and stochastic dynamics in optically excited alkali gases.

Collisional processes involving Rydberg atoms and ions are of interest both as a fundamental problem of modern atomic physics and theory of atomic collisions and also for numerous applications to spectroscopy, kinetics of high and low temperature plasmas and gases, and astrophysics. Atom in Rydberg state consist of a single excited electron (Rydberg electron) far removed from atomic core while the remaining electrons “screen” the nuclear charge. Thus the Rydberg electron moves essentially in a Coulomb field created by the core. An electron in highly-excited orbit is very weakly bound to the core. The energy gap between the adjacent excited states varies as n^{-3} and for atoms in Rydberg states is very small. Therefore, such atoms are influenced extremely strongly even by a weak external perturbation. Under the action of electromagnetic fields or interaction with other atomic particles, Rydberg electron may easily make a transition to other highly excited states or may be separated from the core resulting to the ionisation of the Rydberg atom. Numerous studies [29, 79] of the time evolution of a Rydberg electron moving in a Coulomb potential under the action of a variable field using quasi-classical description were made. These studies revealed that Rydberg electron motion perturbed by this field in the region of highly excited bound states exhibits transition from regular behaviour to chaos as the external fields are increased. As a result of this sensitivity to the external field, the observed behaviour of physical system that exhibit chaos appears to be random, even though the model of the system is 'deterministic' in the sense that it is well defined and contains no random parameters. The highly excited hydrogen atom in a monochromatic field is one of the simplest real non-linear quantum system with stochastic behaviour. The theory of stochastic drift of a Coulomb electron in a microwave

field was developed in the works [29, 30, 31]. In this thesis several methods borrowed from these works were adopted to describe stochastic behaviour of the Rydberg atom in the collisions with the ground state atom in an associative ionization process.

Another important type of energy transfer in vapour cells and plasma is a process when atoms and ions efficiently absorb their own resonance radiation. A photon emitted by an atom within vapour cell will be absorbed and reemitted repeatedly by other atoms before it will escape from the vapour cell. This effect is known as a radiation trapping. The radiation trapping effect is most relevant in spectroscopic experiments where optically thick media are used. Radiation trapping is important in areas as diverse as stellar atmosphere physics [5], plasmas physics, luminescence of atomic vapours [6], optical phenomena in the terrestrial atmosphere, molecular luminescence [7], and cold atom physics [8]. It plays an important role wherever resonant light interaction with atomic vapours occur, whether in spectroscopy, gas lasers, atomic line filters used in optical information transmission, luminescent solar concentrators. Although the most important commercial application where radiation trapping plays an important role are fluorescent lamps. In these lamps the radiation trapping lengthens the effective lifetime of emission as viewed from outside the lamp. The control of this trapping is therefore an important design consideration for low pressure lamps. Electrodeless gas discharge lamps are finding increasing use in lighting applications due to their increased lifetime. In spectroscopic measurements radiation trapping process can influence obtained values of the cross sections, lifetimes and other spectroscopic parameters. The emission and reabsorption process is fundamental to the formation of stellar lines, where it is called radiation transfer. Dark lines in the stellar spectrum observed by Fraunhofer at the early years of spectroscopy resulted from radiation transfer processes. Dense clouds of cold, trapped atoms are also influenced by radiation trapping [8]. The radiation trapping process can be described by the integro-differential Holstein-Biberman equation [9]. Molisch and Oehry [6] have provided a detailed discussion of research on radiation trapping.

Laser excitations of atoms, ions and molecules, absorption and emission processes in vapour cells are usual in modern spectroscopy and plasma physics. Several parameters are commonly used to describe the strength of atomic and molecular transitions. The

Einstein A and B coefficients, f values (also called "oscillator strengths"), photoionization cross-sections and transition dipole moments are some of the parameters that characterize the "strength" of the transition. Optical transition probabilities (Einstein coefficients A) between discrete states and photoionization cross sections are needed for the investigation of the kinetics of excitation, ionization and recombination processes in low-temperature plasmas. Photoinization cross sections, transition probabilities and oscillator strengths for transitions involving high excited electronic states of atoms and ions are often used in astrophysical applications, stellar atmospheres and plasmas (discharges, laser media and flames). Alkali atoms as quasi-one-electron systems have proven to be an important and interesting testing ground for theoretical descriptions of the optical transition processes, both for *ab inito* theories and semiempirical calculations.

One of the simplest photochemical processes is photodissociation, i.e. interaction of a molecule with light, leading to the breaking of a chemical bond. In photodissociation process one selectively excites single vibrational excited state of the molecule. Absorption of the photon in the diatomic molecule leads to the photo fragmentation via metastable molecular state into two separate atoms. This metastable molecular state correlates with the atomic states of both atoms. After the photodissociation in the spectrum of photofragments atomic spectral lines can be observed. Photodissociation process of alkali dimmers are extensively studied in laser spectroscopy experiments. Correlation between the parent molecule's quantum state and the photofragments quantum states distribution permits a detailed description of the excited state potential energy surface and frequently provides information about interactions with other electronic states. Photodissociation reactions of small molecules are not only interesting from the viewpoint of fundamental science, but also have a strong influence on atmospheric and astrophysical processes as example photodissociation regions in the interstellar medium.

Atomic units $\hbar=m_e=e=1$ are used throughout this promotion work, unless specified otherwise.

To solve several of the problems of laser spectroscopy that were mentioned above, in the framework of the present promotion work the following four **tasks** have been set:

1. Development of new theoretical model of ionizing collisions in alkali gases involving Rydberg atoms by taking into account redistribution of population over a range of Rydberg states prior to ionization, which is caused by non-adiabatic processes in overlapping multiple level crossings of quasi-molecular Rydberg states. In addition to the stochastic treatment accounting for the process of *l*-mixing of Rydberg states at large internuclear distances and twisting of the collision trajectories on attractive potentials. Apply this model to calculate the associative ionization rates for $Na^{**}(nl) + Na(3s) \rightarrow Na_2^+ + e$ collisions.

2. Investigation of photoabsorption from the $Na(3p_{3/2})$ state by using model potential method. Calculation of the Einstein coefficients and ionization cross sections for $Na(3p_{3/2})$ atoms. Testing of the accuracy of the calculations, with a variety of model potentials and parameter sets of these potentials.

3. Solving the Biberman-Holstein equation describing radiation trapping in an atomic vapour by the novel analytical method called geometric quantization technique. The treatment is based on considering the integral trapping equation as a wave equation for an associated quasiparticle with a complicated form of its dispersion law. The latter is determined by the spectral properties of the vapour medium. Provement the applicability of geometric quantization technique in more complicated geometries, like elliptical cylinders, and prolate and oblate ellipsoids.

4. Theoretical investigation of the photodissociation process $Na_2(X^1\Sigma_g^+, v'',J'') + h\nu_{458nm} \rightarrow Na_2^*(B^1\Pi_u) \rightarrow Na^*(3p) + Na(3s)$ within the framework of the Born-Oppenheimer approximation. Calculation of the cross sections for the photodissociation of sodium molecule $Na_2(X^1\Sigma_g^+, v'')$ by λ_{PD} = 458 nm radiation from an Ar^+ ion laser for various possible initial vibrational levels v''. Such data were required for interpretation of an imaging experiment with the same photodissociation process.

1. Ionization of Rydberg diatomic quasimolecular complex formed by collisions of alkali atoms

1.1. Introduction

Excitation of Rydberg states in atomic gases is inevitably accompanied by spontaneous ionization due to collisions with the surrounding parent atoms. Three types of atom-atom collision ionization processes can be identified:

$$\begin{aligned} A^* + B^* \rightarrow \quad & A^+ + B^-, && \text{ion pair formation} \\ & A^+ + B + e, && \text{Penning ionization – (PI)} \\ & AB^+ + e. && \text{associative ionization – (AI)} \end{aligned}$$

Ion pair formation takes place in collision of two excited atoms, A^* and B^* due to non-adiabatic transitions between covalent (AB^{**}) and ionic (A^+B^-) terms at large internuclear distances. Penning (PI) and associative (AI) ionization result from autoionization of quasimolecular continuum states (AB^{**}) at small internuclear distances.

In this work we consider AI and PI processes, in which an alkali atom A in the ground state collides with a Rydberg atom $A^{**}(nl)$:

$$A^{**}(nl) + A \quad \begin{cases} \nearrow & A_2^+ + e; \qquad \text{(AJ)} \\ \searrow & A^+ + A + e, \qquad \text{(PJ)} \end{cases} \tag{1}$$

In the AI process the colliding atoms form a molecular bond, which is stabilized by the emission of Rydberg electron. Depending from relative collision energy of the colliding $A^{**}(nl) + A$ system, we can identify in the reaction (1) two distinct channels, AI and PI (see also eq. (6)). The only limitation to energy of collisions (i.e., velocity) that lead to AI ore PI is enforced by the condition that lifetimes of the involved Rydberg states must be larger than the time in which the two colliding atoms reach the (small) internuclear distances, at which covalent molecular Rydberg states cross the state of the molecular ion. This excludes from the group of associatively ionizing media gases cooled to ultracold temperatures, at which collision times exceed the lifetimes of Rydberg states [13].

The main processes leading to the formation of A^+ ions in experiments involving $A^{**}(nl) + A$ collisions are Penning ionization and photoionization by blackbody radiation

(BBR) [publ2]. BBR is always present in experiments. The blackbody radiation photons can penetrate into the reaction zone from, e.g, a hot atomic beam source (oven). BBR induces also transitions between neighbouring Rydberg states and shortens the effective lifetimes [14]. The A_2^+ ions can be created only by the associative ionization. AI possesses the smallest threshold energy among the ionization processes. Most experiments on AI collisions of Rydberg atoms in alkali gases, which are of interest for the present study, have been performed by Weiner (see, e.g., the review by Weiner et al 1990 [3]); the results of other studies are reviewed by Klucharev 1993 [15]. These studies consider associative ionization rates as a function of principal quantum number n under various experimental conditions (thermal gases, single and crossed atomic beams). The first successful theoretical descriptions of the collision processes (1) was developed by Duman and Shmatov 1980 [16], Janev and Mihajlov 1980 [17], and Mihajlov and Janev 1981 [18] and is known as the *linear DSMJ model* (Duman-Shmatov-Mihajlov-Janev). In this approach, the inelastic processes in the colliding system $A^{**}(nl) + A$ are the result of dipole interaction between the excited Rydberg electron and the quasimolecular subsystem $A^+ + A$. The DSMJ model uses the adiabatic approximation and classical description of motion of the colliding nuclei.

The linear DSMJ model uses incorrect assumptions and integration procedures in order to obtain simple analytic formulae. The linear DSMJ model was corrected by Weiner et al 1986 [19] by taking into account the order and limits of successive integrations (strong non-linearity of dipole-dipole interaction). Nevertheless, predictions of this model often strongly deviate from the experimental data [3, 4].

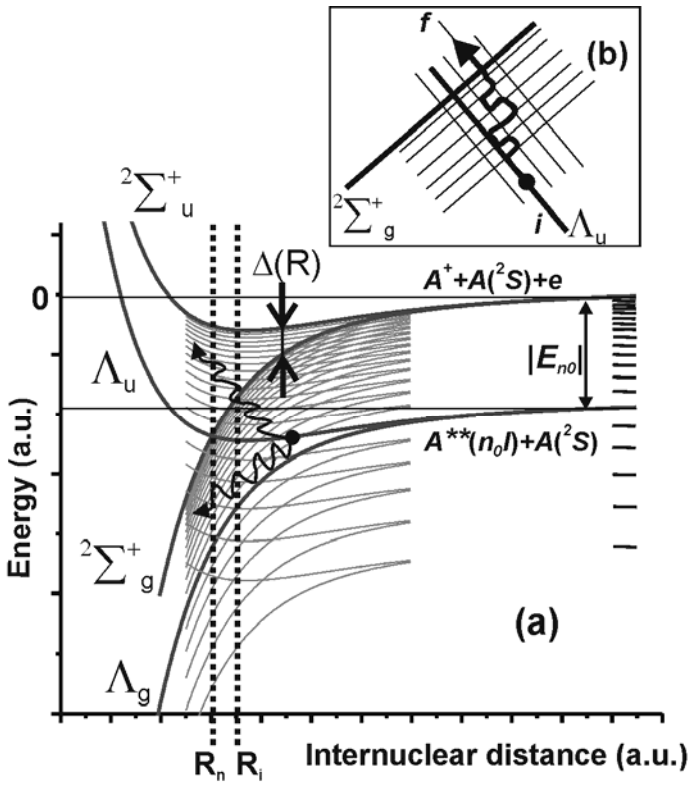

Fig. 1. Schematic illustration of the mechanism of $A^{**}(n_0\ l) + A$ collison process. (a) Quasi-molecular potentials involved in the ionization process. (b) Illustration of Brownian-like migration of the population through multiple level crossings of quasi-molecular Rydberg states.

The observed disagreement can be attributed to the fact that the DSMJ model ignores an important feature in the dynamics of collisions with Rydberg atoms. Namely, it ignores the fact that the colliding pair of atoms coming in along a covalent highly excited molecular potential will pass through numerous crossings with other covalent state of Rydberg series before it will reach the ionic state (see fig. 1.a). Exchange interaction within the $A^+ + A$ quasi-molecular ion splits the electronic states of *gerade* and *ungerade* symmetry by $\Delta(R)$. In fig. 1.a the initial covalent Λ_u state crosses the ionic $^2\Sigma_g^+$ state at the internuclear distance $R = R_n$, becoming autoionizing for $R \le R_n$, while $|E_{n0}|$ denotes the binding energy of Rydberg electron in the initial n_0 state.

In the reality the path by which the population coming in along the initial state (i) reaches the final state (f) in the ionization continuum may be very complicated. Due to nonadiabatic diffusion of Rydberg electron this path resembles a kind of random walk of a Brownian particle in the energy spectrum of Rydberg states (fig. 1.b). Due to this process, the population can migrate from the initial state $\Lambda_u^{(i)}$ to another state $\Lambda_u^{(f)}$ by the

time it reaches the ionic potential $^2\Sigma_g^+$. As a result, the effective internuclear distance of the effective crossing point R_i with the ionic curve is different from the point R_n assumed by the DSMJ model.

The situation is further complicated by the fact that for high Rydberg states the neighboring zones of non-adiabatic transitions between covalent Rydberg states overlap. The latter makes it impossible to treat the collision process as a sequence of separate Landau-Zener non-adaibatic transitions redistributing the population flow in the initial state *i* over a number of final states *f*. Instead, the process may be considered in terms of stochastic migration of Rydberg electron in the energy spectrum of Rydberg quasi-molecule by applying the elements of chaos theory [20].

The present study is an effort to develop an alternative to Landau-Zener treaty allowing a reliable theoretical description of ionizing collisions involving Rydberg atoms. This needs performing essential modifications of the non-linear DSMJ model, which can be listed as follows:

1) **account for the influence of *twisting effect* [21] on the efficiency of AI channel We consider an additional potential barrier caused by the centrifugal part of the effective potential at large internuclear distances;**
2) **we account for passage of the colliding complex through a zone of multiple overlapping level crossings by treating the dynamics using the stochastic theory [20,22,publ1] as described in this work;**
3) **in this approach we take into account the process of *l*-mixing of Rydberg states at large internuclear distances [23].**

In this work stochastic theory was developed and applied to alkali atom (Rb, Na) collisions [publ1, publ3, publ4]. This is an original theory that has not yet been used by other authors to describe collisional ionization processes.

1.2. Non-linear DSMJ model

The main simplication that allows the probability of the reaction (1) to be described analytically exploits the possibility to restrict the analysis to the range of internuclear distances *R*, in which the highly excited RE electron is common for both colliding nuclei. At such distances a quasi-molecular ion A_2^+ is formed (fig. 2). Charge exchange

between both nuclei of the $A^+ + A$ of the quasi-molecular ion A_2^+ causes inner-shell electron localization changes from one nucleus to another. Such oscillating dipole generates a quasi-monochromatic electromagnetic field, which can induce a dipole transition of the Rydberg electron to the continuum.

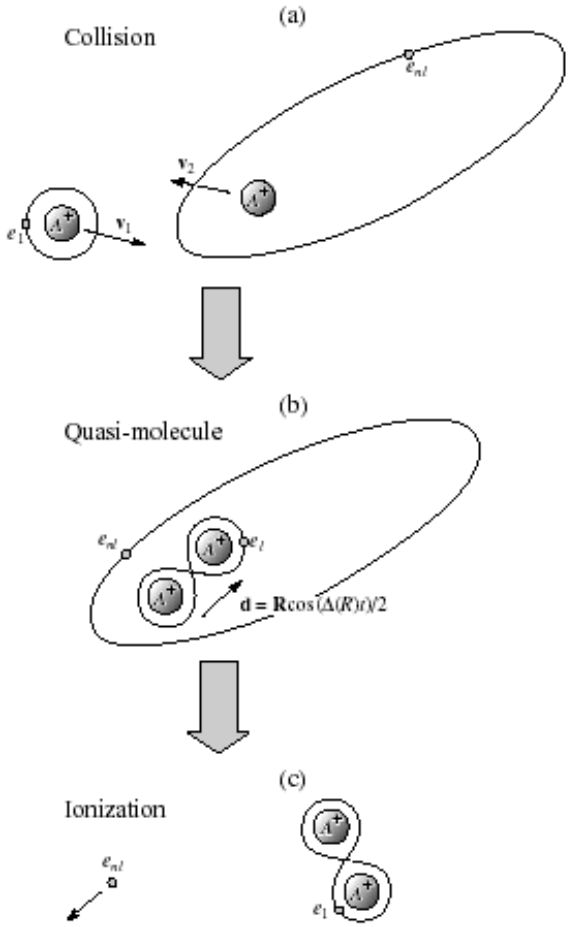

Fig. 2. a) Ground state atom A collides with a Rydberg atom $A^{**}(n_0\ l)$. b) A short lived molecular state in which the RE e_{nl} becomes commom for both nuclei, is formed during the collision. Both atomic ions of the quasi-molecular complex A_2^+ exchange with the inner valence electron e_1 to produce a variable dipole moment $\vec{d}$, which oscillates at the exchange interaction frequency $\Delta(R)$. (c) Interaction of the weakly bound RE with the internal diplole electric field causes its detachment from the quasi-molecular ion.

The assumption that motion of the Rydberg electron is decoupled from the motion of heavy particles allows the approximation of energies of the colliding $A^{**}(nl) + A$ system by the potentials of A_2^+ ion by subtracting from them the binding energy $|E_n| = 1/(2n_{eff}^2)$ of the Rydberg electron (fig. 1.a). The effective quantum number n_{eff} relates to the principal quantum number n via the quantum defect μ_l: $n_{eff} = n - \mu_l$.

The potentials $V_u^+(R)$ and $V_g^+(R)$ of the molecular ion A_2^+ (corresponding to the repulsive $^2\Sigma_u^+$ and the attractive $^2\Sigma_g^+$ potentials, respectively, see fig. 1.a, are described by the asymptotic equation [18, 24, 25]:

$$V_{u,g}^+(R) = \frac{1}{2}\left[-\frac{\alpha}{R^4} \pm \Delta(R)\right]. \qquad (2)$$

Here, the signs "+" and "–" corresponds to the potentials V_u^+ and V_g^+, respectively, α is the polarizability of the colliding atom A in the ground-state, and $\Delta(R)= V_u^+ - V_g^+$ (see fig 1.a) is the exchange interaction energy. It can be described by an analytical form [18, 24, 25]:

$$\Delta(R) = BR^{(2/\gamma)-1}\exp(-\gamma R), \qquad (3)$$

Parameters B and γ are determined by the asymptotic properties of wave function of the inner electron in the field of the atomic ion A^+. The corresponding potentials of the A_2^{**} quasi-molecule are obtained from Eq. (2) as $V_u = V_u^+ - |E_n|$ and $V_g = V_g^+ - |E_n|$. Exchange interaction within the molecular ion is equal to the binding energy of Rydberg electron at the critical internuclear distance R_n:

$$\Delta(R_n) = |E_n| = \frac{1}{2n_{eff}^2}. \qquad (4)$$

Ionization occurs if system reaches the internuclear distance $R<R_n$, where the energy associated with the oscillating dipole $\hbar\omega(R)= \Delta(R)$ exceeds the binding energy $|E_n|$ of the Rydberg electron.

The incoming potential V_u acquires the autoionization width [17, 18]

$$W(R) = cR^2\omega^3(R)\,\sigma_{ph}\big(\omega(R)\big)\big/8\pi, \qquad (5)$$

where $\sigma_{ph}(\omega(R))$ is the photoionization cross section of Rydberg atom, and c is the speed of light.

The collison process can branch into associative and Penning ionization channels (1). Depending from the relative kinetic energy $E=E(R\to\infty)$ of the colliding nuclei, the closest possible internuclear distances that can be reached by the colliding nuclei are different. PI or AI processes were restricted to different ranges of internuclear distances:

$$\begin{cases} R \geq R_1 \Rightarrow \text{Penning ionization;} \\ R < R_0 \Rightarrow \text{associative ionization,} \end{cases} \qquad (6)$$

where R_1 and R_0 are defined by:

$$E = \Delta(R_1) \qquad \text{and} \qquad \begin{cases} R_0 = R_1, & \text{if } E > |E_n|; \\ R_0 = R_n, & \text{if } E \le |E_n|. \end{cases}$$

The cross section σ_{AI} of the AI process is determined by the ionization probability P_{AI}. For a given initial collision energy E, the cross section is obtained by integrating the probability over the range of those impact parameters ρ, which allow the colliding nuclei to reach the internuclear distance R_0 [19]:

$$\sigma_{AI}(E) = 2\pi \int_0^{\rho_{\max}} P_{AI}(\rho, E)\rho \, d\rho \, . \tag{7}$$

The probability P_{AI} depends on the given initial molecular potential $V_u(R)$, the distance-dependent collision velocity $\upsilon_r(R)$, and the autoionization width $W(R)$. This dependence for P_{AI} was derived in our work [publ3]:

$$P_{AI}(\rho, E) = \exp\left(- g\theta(R_n - R_1)\int_{R_1}^{R_n} \frac{W(R)}{\upsilon_r(R)} dR \right)\left[1 - \exp\{-2g\int_{R_m}^{R_0} \frac{W(R)}{\upsilon_r(R)} dR\} \right]; \tag{8}$$

$$\upsilon_r(R) = \sqrt{\frac{2}{\mu}\left(E - V_u^{+}(R) - E\frac{\rho^2}{R^2} \right)}, \tag{9}$$

where g = ½ is the statistical factor describing the probability that the colliding system will evolve along the repulsive potential V_u to the turning point R_m . The quantity μ is the reduced mass of both colliding atoms, and $\theta(x)$ is the Heaviside function with the properties:

$$\begin{cases} \theta(x \ge 0) = 1; \\ \theta(x < 0) = 0. \end{cases}$$

If $E_1 < E_n$, then probability of Penning ionization becomes $P_{PI}=0$ and the total probability $P_0 = P_{AI} + P_{PE}$ becomes equal to the probability of AI:

$$P_0(\rho, E) = 1 - \exp\left[- 2g\int_{R_m}^{R_n} \frac{W(R)}{\upsilon_r(R)} dR \right].$$

The linear DSMJ model uses only the linear part of this equation. The largest possible impact parameter ρ_{max}, for which the AI is still possible, is the one for which R_0 coincides with the turning point R_m, i.e when R_0 satisfies the condition $\upsilon_r(R_0) = 0$.

Finally, if the temperature T can be defined, the collision rate is given by:

$$k_{AI} = \int_{E_{\min}}^{\infty} \sigma_{AI}(E)\left(\frac{2E}{\mu}\right)^{1/2} f(E,T)dE\,. \qquad (10)$$

where $f(E,T)$ is the collision energy distribution for each particular experiment. The lower integration limit is the collision energy required to reach R_0:

E_{min}= max[$V_u(R_0)$ +|E_n|, 0].

The energy $E_{\min}$=0 is chosen if $V_u(R_0) < 0$ (attractive potential) and that means that the nuclei can reach the internuclear distance R_0 at small initial energies $E_{\min} \to 0$.

For nl states of alkali atoms with $l \geq 2$, the l-mixing process should be taken into account and formula (10) must be modificed. For these l-states the l-mixing cross sections are close to geometrical cross sections of Rydberg atoms, and therefore l-mixing is stronger for $l \geq 2$ states than for nS states. The processes of l-mixing typically proceed at large internuclear distances $R_{mix} \approx \langle r \rangle_n = 3n^2_{\text{eff}}/2$ [23]. Here $\langle r \rangle_n$ is the mean value of Rydberg electron distance from nuclei at $n_{eff} >> l$. At the same time, the typical internuclear distances, at which the collisional ionization of Na atom takes place, are only about 10-15 a.u. Therefore it is reasonable to assume that a complete l-mixing has taken place by the time when the colliding atoms have reached the ionizing internuclear distances. Hence, the total rate constant should be calculated by summing the contributions $k_{AI}(n,l')$ of individual l'-states:

$$k_{AI}^{total}(n) = \frac{1}{n^2}\sum_{l'=0}^{n-1}(2l'+1)\,k_{AI}(n,l')\,. \qquad (11)$$

1.3. Collision velocity distributions

In experiments the reaction rate constants (10) and not the cross sections are measured (see for example [3, 15]). In order to compare our theoretical model with experimental results we must to know the collision energy or velocity distribution (fig.

3). The energy distribution *f(E,T)* relates with the velocity distribution as $f(E,T) = \mu^{-1}\upsilon_c^{-1}F(\upsilon_c,T)$.

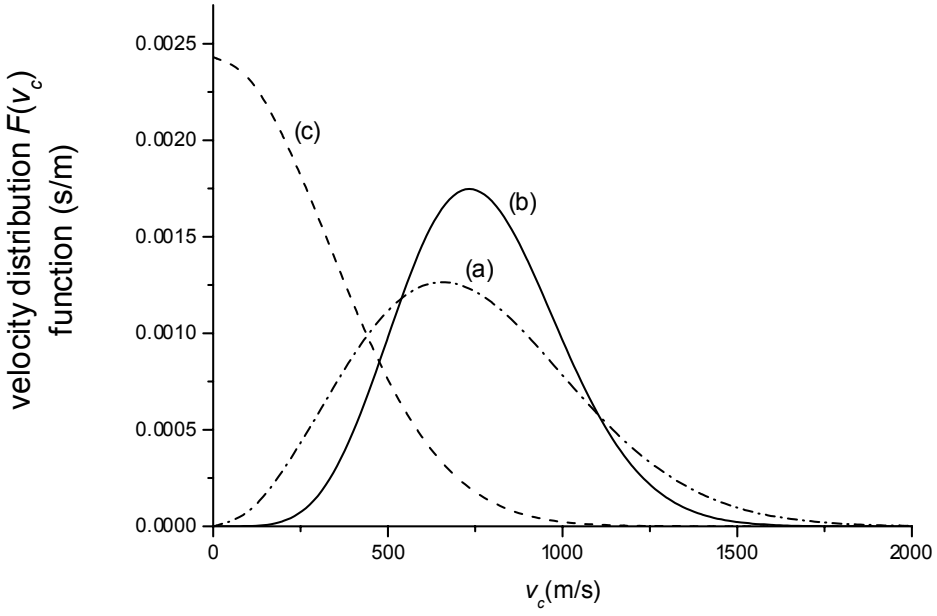

Fig.3. Relative collision velocity distribution of Na atoms in (a) thermal sodium vapours in a gas cell at T=600K, (b) two orthogonally crossed effusive beams of sources, at T_{ef}=600K, (c) single effusive beam with source at temperature T_{ef}=600K.

In a gas cell at temperature *T*, this distribution is given by the Maxwell function (fig. 3.a):

$$F_{Maxwell}(\upsilon_c) = \sqrt{\frac{2}{\pi}}\left(\frac{\mu}{T}\right)^{\frac{3}{2}}\upsilon_c^2 \exp\left(-\frac{\mu\upsilon_c^2}{2T}\right), \tag{12}$$

where $\upsilon_c = \sqrt{2E/\mu}$ is the collisional velocity. For two crossed effusive atomic beams with sources at temperature T_{ef} the distribution is given by (fig. 3.b):

$$F_{cb}(\upsilon_c) = \upsilon_c^5\left(\frac{\mu}{T_{ef}}\right)^3 \exp\left(-\frac{\mu\upsilon_c^2}{T_{ef}}\right). \tag{13}$$

The distribution for head-tail collisions within a single effusive beam is given by (fig. 3.c):

$$F_{sb}(\upsilon_c) = 2\left(\frac{\mu}{\pi T_{ef}}\right)^{1/2} \exp\left(-\frac{\mu\upsilon_c^2}{T_{ef}}\right) \tag{14}$$

We can rewrite the distribution function in a more general form depending from the beam parameter λ:

$$F^{(\lambda)}(\upsilon_c) = \upsilon_c^{\lambda} \frac{2(\mu / T_{ef})^{\frac{1+\lambda}{2}}}{\Gamma\left(\frac{1+\lambda}{2}\right)} \exp\left(-\frac{\mu \upsilon_c^2}{T_{ef}}\right),$$

where Γ is the gamma function. For λ =0 and λ =5 this distribution $F^{(\lambda)}(\upsilon_c)$ coincides with the single-beam and cross-beam distributions, respectively.

As can be seen from fig. 3, the distribution function for single-beam collision is strongly different from those for crossed beams and vapour cell (see fig. 3, curve c and curves b, and a). In the case of single-beam collisions the main contribution to the integral (10) is due to collisions at small velocities. Therefore, in this case λ =0, and twisting effect must be taken into account. Due to twisting effect, at sufficiently large impact parameters the colliding atoms cannot overcome the potential barrier built by centrifugal forces at large internuclear distances. At small impact parameters, in contrast, the atoms easily pass over the (low) barrier. For a given collision energy E, the critical value of impact parameter $\rho = \rho_{twist}$, for which the radial velocity of the colliding atoms turns to zero on the top of the effective potential $U_{eff}(R) = -\alpha/(2R^4) + E\rho^2/R^2$ (see fig. 4), can be obtained from the equation system

$$\begin{cases} \mathrm{v}_r(\rho, E, R) = 0; \\ \dfrac{\partial \mathrm{v}_r(\rho, E, R)}{\partial \mathrm{R}} = 0. \end{cases} \quad \rightarrow \ \rho_{twist} = (2\alpha / E)^{1/4}$$

The potential barrier limits the range of impact parameters that can bring atoms A^{**} and A to distances as small as R_n.

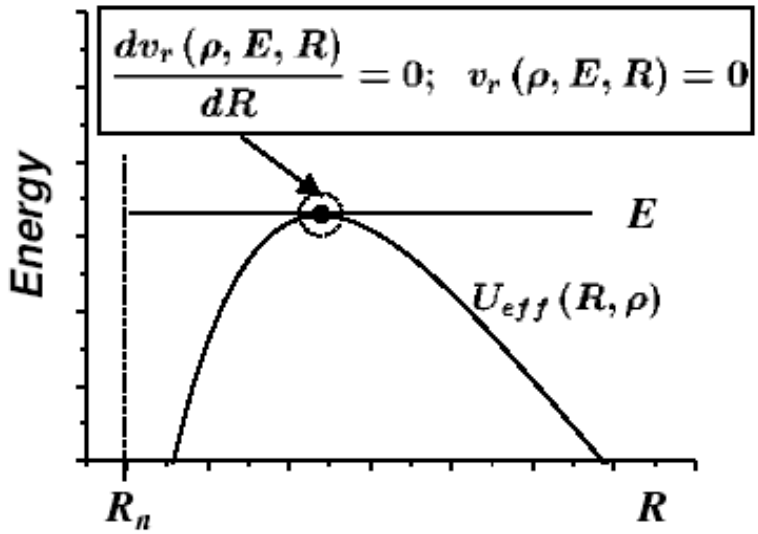

Fig. 4. Passage of the $A^{**} + A$ colliding system over the potential barrier of the effective potential U_{eff}, created by centrifugal forces.

1.4. The theory of Rydberg electron migration

As mentioned in sect. 1.2. (see also fig. 2), the electric dipole field, which is generated by the quasi-molecular ion A_2^+ and which oscillates at the frequency $\Delta(R)/\hbar$, causes a strong coupling of Rydberg electron (RE) to the internal dipole of the ionic core of the quasi-molecule $A^{**}(nl) + A$. Ionization of RE by this dipole electric field occurs as soon as the colliding nuclei reach the threshold distance R_n. Non-adiabatic transitions at multiple level-crossings lead to changes of the effective threshold distance R_i of the ionization (fig. 1), which can become larger than the threshold distance R_n. The conventional Landau-Zener approximation, which assumes that all crossings are isolated from each other, breaks down for Rydberg states due to their characteristically high densities of energy levels. An alternative approach to the treatment of multiple level crossings was proposed by the authors of [26, 20, 22], who explored the applicability of the concept of dynamic chaos [27, 28] to the description of dynamics of RE.

From the point of view of nonlinear mechanics, each level crossing corresponds to a dynamic resonance experienced by the Rydberg electron driven by the internal dipole electric field [26]. Some overtones $k\omega_n$ (where k is an integer) of the frequency $\omega_n = 1/n^{*3}$, with which the RE moves on its Kepler orbit, can coincide with the charge transfer frequency within the A_2^+ core:

$k\omega_n = \Delta(R)$.

If the perturbation of Rydberg electron by internal dipole electric field is sufficiently strong, then the resonances between the neighbouring energy levels overlap. Such overlap in accordance with Chirikov's criterion results in the onset of global chaos [27] in the classical motion of RE.

1.4.1. Diffusion equation

Importantly, the onset of global dynamic chaos exhibits the distinct features of a threshold process on the intensity I_{int} of the internal dipole electric field. The RE motion perturbed by this field in the region of highly excited bound states with effective quantum numbers $n^* > N_{Chaos}$ (see eq. (23) below) becomes unstable: the stochastic layers are combined into a stochastic "sea". In this case, the RE evolution acquires properties characteristic of the so-called K-systems, i.e., strongly locally unstable Hamiltonian systems with intense trajectory mixing in phase space and with rapid uncoupling of correlations between angular dynamic variables. The chaotic motion of Rydberg electron under such conditions may be described with a kinetic equation and its solution yields a time dependent distribution $f(n_{eff}, t)$ of population over Rydberg states. Under the conditions assumed by the adiabatic approximation (the accuracy and limitations of this approximation are analysed in [publ2]), electronic motion adiabatically adjusts to the comparatively slow variation of nuclear configuration in the course of the collision. In that case, we can use the theory of stochastic drift of a Coulomb electron in a microwave field [29, 30, 31] to describe the population distribution $f(n_{eff},t)$ within the region Ω_{chaos} in the n_{eff}-space, where the motion of Rydberg electron is chaotic. Kinetic description time evolution of the Rydberg electron in the reaction (1) can be described using a Fokker-Planck type equation, as suggested in [20]:

$$\frac{\partial}{\partial t} f(n_{eff}, t) = \frac{\partial}{\partial n_{eff}} j \; ; \tag{15}$$

$$j = D(n_{eff}, R(t)) \frac{\partial f(n_{eff}, t)}{\partial n_{eff}} . \tag{16}$$

Here, j is the diffusion flux and D is the diffusion coefficient. For hydrogen atoms:

$$D(n_{eff}, R) = n_{eff}^3 \, \widetilde{D}(R); \quad \widetilde{D}(R) = 0.023 \, R^2 \Delta^{8/3}(R) \left[1 + 1.18 \, \Delta^{2/3}(R) \, L^2 \right]. \qquad (17)$$

Formula (17) was derived by assuming a uniform RE distribution over Zeeman sublevels $m = -l,....,l$. The parameter L is equal to the quasi-classical orbital angular momentum, $L = l + 0.5$. The time dependence of $R(t)$ is determined in the same way as in the DSMJ model (see eq. (3)) Therefore, the diffusion coefficient is a time-dependent variable. The authors of [22] generalize the relation (17), applying the Kepler map technique [32] by accounting the quantum defect, which introduces new features into the pattern of chaos onset.

$$\widetilde{D}(R) = \frac{\omega^4 R^2}{48\pi} \sum_{\Delta l = \pm 1} L_c^4 \, D_{\Delta l}^2(\omega); \qquad (18)$$

$\omega = \Delta(R)$, $L_c = l + 0.5 + \Delta l/2$;

$$D_{\Delta l}(\omega) = \left[-\frac{\sin(\pi \, \Delta\mu)}{2} - \frac{\sqrt{\pi}}{x} \Phi'_{\Delta\mu}(x) + \Delta l \sqrt{\frac{\pi}{x}} \, \Phi_{\Delta\mu}(x) \right]; \qquad (19)$$

$x = (\omega L_c^3/2)^{2/3}$.

The dependence of $D_{\Delta l}(\omega)$ over $\Delta(R)$ is expressed in terms of the standard Airy function $\Phi_{\Delta\mu}$ and its first derivative [29]:

$$\Phi_{\Delta\mu}(x) = \frac{1}{\sqrt{\pi}} \int_0^\infty \cos\left(x\xi + \xi^3/3 + \pi\Delta\mu \right) d\xi,$$
$$\Phi'_{\Delta\mu}(x) = \frac{d}{dx} \Phi_{\Delta\mu}(x) \qquad (20)$$

The behavior of $\widetilde{D}(R)$ can change significantly different for states with different angular momenta l because of difference of the quantumdefects, $\Delta\mu = \mu_{l+\Delta l} - \mu_l$, between l and $l + \Delta l$ Rydberg series. Equations (18)-(20) were derived using the dipole matrix element between bound states nl and $n'l'$ with $E_{n'} = E_n \pm \omega$ represented in the semi-classical form [33]. For hydrogen-like levels with $\mu_l = 0$, the relation (18) becomes equal to eq. (17). The autoionization width $W(R)$ of the incoming repulsive $^2\Sigma_u^+$ potential curve (5) can also be calculated using a similar approach. The obtained result is:

$$W(R) = \widetilde{W}(R) \big/ n_{eff}^3; \qquad (21)$$

$$\widetilde{W}(R) = \frac{\omega^2 R^2}{12\pi} \sum_{\Delta l=\pm 1} \frac{L_c^5}{l+0.5} D_{\Delta l}^2(\omega) . \qquad (22)$$

1.4.2. Boundary conditions

For the stochastic instabilities to develop it is necessary that the intensity I_{int} of the internal dipole electric field exceeds some certain critical value. This value corresponds to the interval of binding energies of Rydberg electrons, within which the dynamic resonances overlap, i.e. the stochastic layers are combined into a stochastic "sea" The standard mapping [27,28,32] and the Chirikov's criteria [22] for the onset of global chaos allowed the determination of region $N_{chaos}(R) < n_{eff} < N_{auto}(R)$ in the energy space (ε=-1/(2 n^2_{eff})), within which the diffusion of Rydberg can occur via that stochastic "sea". The lower boundary value $n_{eff} = N_{chaos}(R)$ is determined from the Chirikov's criteria [22] as:

$$N_{chaos}^5(R) = \frac{1}{12\pi\omega\sqrt{2\pi\widetilde{D}(R)}} , \qquad (23)$$

The region of low –lying states ($n_{eff} < N_{chaos}(R)$) is characterized by large energy spacing between the neighboring levels, such that the diffusions process in this region is forbidden. Random walk over n_{eff} can not penetrate into the region $n_{eff} < N_{chaos}(R)$. Hence $n_{eff} = N_{chaos}(R)$ specifies the position of a reflecting "wall", beyond which the diffusion flow is not possible: $j(n_{eff}=N_{chaos}) = 0$. The channel of ionization is open for highly excited states with $n_{eff} > N_{auto}(R)$ for which the frequency of the internal electric dipole field $\hbar\omega(R) = \Delta(R) > 1/2n_{eff}^2$:

$$n_{eff} > N_{auto}(R) = \frac{1}{\sqrt{2\omega(R)}} \qquad (24)$$

Beyond $N_{auto}(R)$, the Rydberg level ionizes at the rate $W(R)$. This ionization process can be described by the DSMJ model (eq. (8)).

1.4.3. Effective collision and diffusion times

It is useful to introduce the effective time $\tilde{t}(R)$. This allows one to make a substitution of a form $d\tilde{t} = dt\,\tilde{D}(R)$ (see eq. (18)). Dividing both sides of eq. (15) by $\tilde{D}(R)$, we can modify it to the form:

$$\frac{\partial}{\partial \tilde{t}} f(n_{eff}, \tilde{t}) = \frac{\partial}{\partial n_{eff}} \left\{ D_{stat}(n_{eff}) \frac{\partial}{\partial n_{eff}} f(n_{eff}, \tilde{t}) \right\}, \qquad (25)$$

where $D_{stat}(n_{eff}) = n_{eff}^3$ is the stationary diffusion coefficient. The effective collision time along a classical trajectory $R^{(u)}(t)$ of the nuclei moving on the potential V_u with the radial velocity υ_r is:

$$\tilde{t}(R) = \int_R^\infty \frac{dR^{(u)}}{\upsilon_r(R^{(u)})} \tilde{D}(R^{(u)}) \theta\left(n_{eff,0} - N_{chaos}(R^{(u)})\right),$$

The effective collision time $\tilde{t}(R)$ within the zone of regular motion $n_{eff,0} < N_{chaos}(R)$ becomes equal zero because there is no diffusion in this region.

It is possible to introduce the effective diffusion time, $\tau_{diff}(R)$, which is the time needed for Rydberg electron to migrate from the initial state $n_{eff,0}$ to the autoionization boundary $N_{auto}(R)$. Due to the fact that there are no level crossings in the autoionization zone $n_{eff} > N_{auto}(R)$ (see fig. 1), no population diffusion occurs in this region and $\tau_{diff}(n_{eff,0} = N_{auto}) = 0$. The additional condition $\partial \tau_{diff}(n_{eff,0} = N_{auto}) / \partial n_{eff,0} = 0$ takes into account the reflection of the diffusive population flux in Rydberg states from the boundary with zone of regular motion $n_{eff} < N_{chaos}(R)$, and it represents the above mentioned boundary condition $j(n_{eff}=N_{chaos}) = 0$. In [publ3], the following expression for the effective diffusion time $\tau_{diff}(R)$ is derived:

$$\tau_{diff}(R) = 4.5 \frac{\left(n_{eff,0} - N_{auto}(R)\right)^2}{2 n_{eff,0} N_{auto}^2(R)}. \qquad (26)$$

Our calculation method is based on the comparison of the effective collision time and the effective diffusion time. If $\tilde{t}(R) > \tau_{diff}(R)$, the collision time is sufficiently long to allow the population to diffuse and to reach the autoionization boundary $N_{auto}(R_i)$ at the distance $R_i(\rho, E)$ (see fig. 1):

$$\tilde{t}(R_i) = \tau_{diff}(R_i)\,. \qquad (27)$$

The probability $P_{AI}(\rho, E)$ of AI reaction can now be found using eq. (8) and replacing the crossing point R_n with $R_i(\rho,E)$, which corresponds to $n_{eff,i}(\rho,E)=N_{auto}(R_i)$. The AI rate constant can be found from eq. (10) by using the cross section $\sigma_{AI}(E)$ given by eq. (7) .

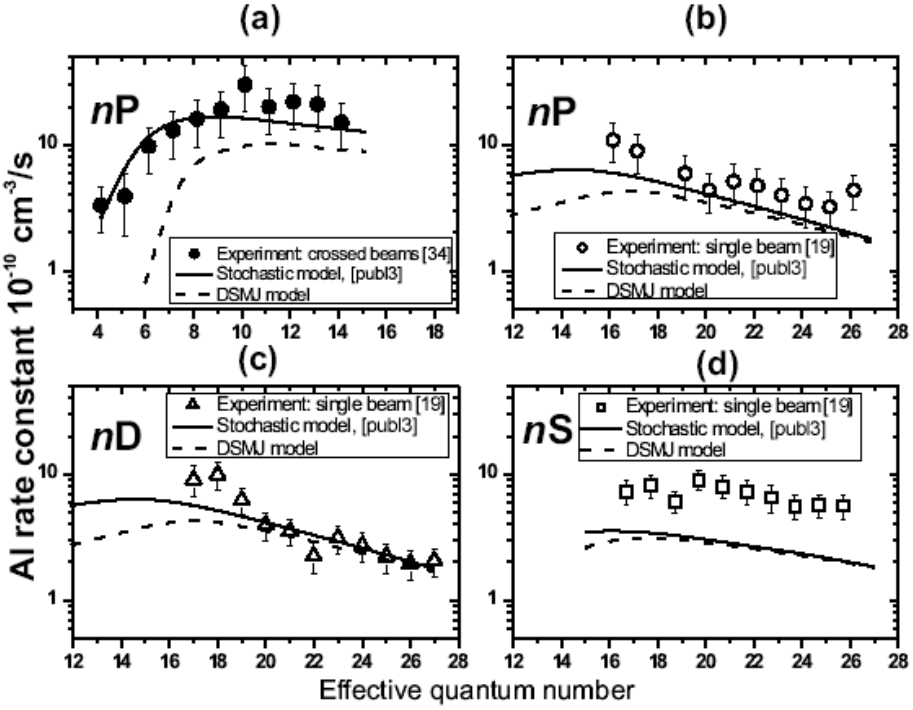

Fig. 5. Experimental and theoretical $Na^{**}(nl)$ + Na AI rate constants. (a) $Na^{**}(n\mathrm{P})$ states: crossed beam experiment [34]; (b) $Na^{**}(n\mathrm{P})$ states: – single beam experiment [19]; (c) $Na^{**}(n\mathrm{D})$ states: single beam conditions [19]; (d) $Na^{**}(n\mathrm{S})$ states: single beam conditions [19]; solid curves – stochastic theory; broken curves - DSMJ model.

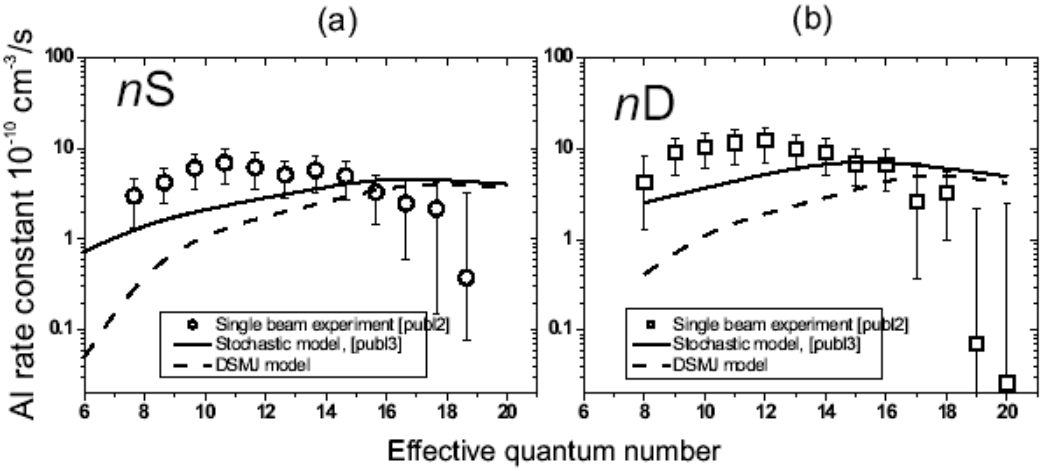

Fig. 6. Recalculated Rate constants of AI in $Na^{**}(n\mathrm{S}, n\mathrm{D})$ + Na sub-thermal collisions in a collimated effusive beam from source at T_{ef} = 635 K (see discussion in the text). (a) circles - experiment, *n*S states [publ2]; full curve - stochastic model, broken curve - DSMJ model. (b) squares - experiment, *n*D states [publ2]; full curve – stochastic model; broken curve - DSMJ model.

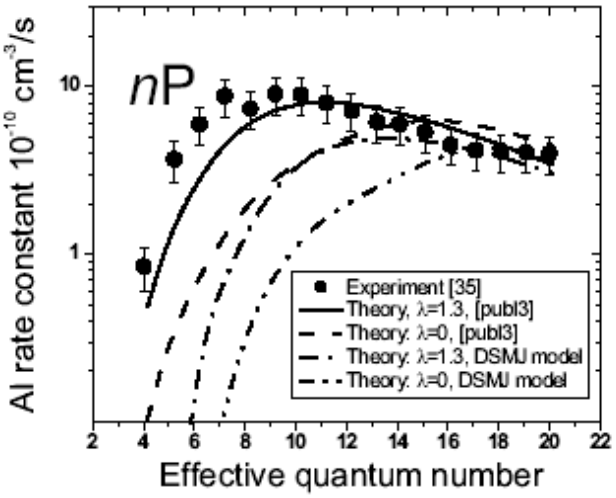

Fig. 7. Rate constants of AI in $Na^{**}(n\mathrm{P}) + Na$ collisions in a single effusive beam from source at T_{ef} = 700 K: circles – experiment [35]; full curve - stochastic model with collimation parameter λ = 1.3; broken curve - stochastic model with λ = 0; chain curve - DSMJ model with λ = 1.3; double dotted chain curve – DSMJ model with $\lambda = 0$.

1.5. Associative rate constants for $Na^{**}(n\mathrm{S,P,D})$ states

The above theory of collisional ionization was used to calculate the AI rate constants k_{AI} for the conditions of available experimental studies. Stochastic theory works well in the case of thermal collisions in crossed beams, and the same can be expected under vapour cell conditions. Fig. 5 shows the experimental results on k_{AI} measured for $Na^{**}(nS,\mathrm{P,D})$ states in the crossed beam experiment [34] (fig 5.a) and in the single beam experiment [19] (fig. 5.b,c,d), as compared with our calculations. In fig. 6 and 6 our theoretical data is compared with the experimental data of [publ2] and [35], respectively. Note, that the single beam data of [19] is relative, and the authors obtained absolute scaling by joining these data with the absolute crossed beam results of [34]. This procedure is not well justified and can cause systematic errors. In the experiments of [34] effusive beams at temperature of 600 K were used, whereas the experiments of [19] were performed at 1000 K.

In the crossed beam experiment [34] the Na_2^+ ions are produced not only due to the collisions of $Na^{**}(nl)$ and Na(3S) atoms belonging to different beams, but also due to collisions of atoms belonging to the same beam. Hence the measured rate constant $k_{AI}^{\exp}$ is a sum of crossed beam (k_{AI}^{cb}) and single beam (k_{AI}^{b}) rate constants: $k_{AI}^{\exp} = k_{AI}^{\Sigma} = k_{AI}^{cb} + k_{AI}^{b}$.

The dashed line on fig. 6.a shows the n_{eff} dependence of the total rate constant k_{AI}^{Σ} calculated using the non-linear DSMJ model. One can see that at low effective quantum numbers $n_{eff} < 15$ the stochastic model is in better agreement with experimental data than the DSMJ model. The results of the stochastic theory and the DSMJ model practically coincide for $n_{eff} > 20$. A significant disagreement between the experiment and the theory for *n*S states in a single beam is observed (fig. 5.d). At the same time, rate constants for *n*D in single beam collisions are larger than those for *n*S states (fig. 6). This allows us to presume that the disagreement is caused by incorrect determination of the absolute experimental rate constant values in [19].

Experiments with *n*S and *n*D states of Na are reported in [publ2]. In this paper, the collisional and thermal ionization of sodium *n*S and *n*D Rydberg atoms with n =8–20 has been studied using single effusive atomic beam at the source temperature T=635 K. Number density n_{3S} of the ground-state Na(3S) atoms in the beam was calculated from the geometry of the effusive beam and Nesmeyanov's formula [36]. In fig. 6, the corrected AI rate constants of paper [publ2] are shown. The correction is made using the alternative formula of Browning and Potter [37], which gives approximately two times higher density n_{3S} for the same temperature, and we believe it is more accurate. Good agreement of absolute values, but significant disagreement in shapes between the experimental data and the stochastic model is observed. Since the experiment utilized a well collimated effusive beam, the velocity distribution in atomic beam is close to a beam with parameter λ=0 (14), which was used in the calculations. In addition, the effect of population redistribution by BBR for the *n*S and *n*D states (fig. 6) was taken into account quantitatively as described in [publ3]. For single beam, the main contribution to the AI rate constants is due to collisions of low velocities (fig. 3). One of the possible reasons for such disagreement in shapes is that the present stochastic model may be inapplicable for slow collisions. For slow collisions, the kinetic energy of the colliding pair is lower than the energy separation between adjacent Rydberg states: $\Delta E_n = 1/n_{eff}^3$. For example, for the effusive single beam used in [publ2] the collision energy is smaller the energy separation of Rydberg states with $n_{eff} > 15$, but in the cross beam experiment [34] it is true for $n_{eff} > 7$. The stochastic changes in the quantum state of the Rydberg electron lead to changes in forces acting on the colliding nuclei, and they may noticeably affect

trajectories of the nuclei if the collisions are sufficiently slow. Such randomization of nuclear motion was disregarded in the present calculations. Therefore, instead of using Newton equations for n_{eff} <15 (fig. 6), one should rather treat the nuclear motion in close connection with the dynamics of Rydberg electron and describe the action of random forces on the colliding nuclei using Langevin-type equations.

In fig. 7, the data of the single beam experiment [35] at T_{ef} = 700 K is shown. If the rate constant (10) is calculated using the velocity distribution function (14) with λ = 0, the theoretical rate constants do not agree with the experimental results. If, however, the calculations are done with λ = 1.3, which corresponds to poor collimation (as was the case in the experiment), then a better agreement with the experiment is obtained.

1.6. Conclusion

The main result of papers [publ1, publ3, publ4] is the demonstration that the motion of a highly excited valence electron in the short-lived quasi-molecular system produced by colliding atoms is stochastized. Essential improvement of the DSMJ model describing ionization in collisions with Rydberg atoms and ground-state atoms was achieved. The approach developed in this thesis work includes the stochastic description of motion of Rydberg electron during the collision process. A good agreement was found between the results of the stochastic theory and the experiments in the case of associative ionization in $Na^{**}(nP)$ + Na collisions at thermal collision energies. It was shown that the stochastic model and the DSMJ model converge at large n, but at low n the stochastic model yields a substantially better agreement with the experimental data than the DSMJ model. The choice of the collision velocity distribution is also shown to be important. In the experiments in single effusive beams centrifugal twisting effect must be taken into account to describe the motion of nuclei at low velocities. Effects of collisional l-mixing and BBR-induced transitions as well as the spontaneous mixing of Rydberg states were taken into account, and the conditions ensuring the validity of the adiabatic approximation in the stochastic and DSMJ models were found. This presented analysis allowed to us determine the range of the effective quantum numbers n_{eff}, for which both models can be applied. The theory must be further developed to account for slow atomic collisions, in which randomization of the nuclear motion can become important.

2. Photoexcitation of Na($3p_{3/2}$) to high Rydberg states and photoionization

2.1. Introduction

Spontaneous Einstein coefficients from high lying states or transition probabilities to high lying states and photoionization cross sections are not unambiguously established even for such well known element as sodium, when it concerns the uncertainties of the calculated or experimental values.

In order to calculate transition probabilities and photoionization cross sections, one has to calculate the corresponding transition dipole moments. In the case of alkali atoms it is done by solving the Schrödinger equation for the valence electron in the field of nucleus and the core electrons. In the early works, like Bates-Damgaard [38], authors used quantum defect theory, also known as Coulomb approximation (CA), which neglects the contribution of small radius (outside the core) and is valid for $n_{eff} > l+1$, where n_{eff} and l are the effective principal quantum number and the angular momentum quantum number, respectively.

For the Li, Na, K, Rb, and Cs atoms dipole transition probabilities, oscillator strengths and lifetimes derived from a numerical Coulomb approximation have been investigated in [39] for states with $n \leq 12$, $l \leq 4$. In this approximation, the wave functions are obtained numerically by direct inward integration of Schrödinger equation starting with correct asymptotic boundary conditions. The integration is terminated at a certain small distance r_{cut}, so that the wave function is normalized to unity and the obtained expectation value $\langle r \rangle$ agrees with the Hydrogenic formula for n_{eff}.

In seventies of the last century, further step towards improvement of the quality of calculations beyond the CA was made by accounting for the electron-core penetration, the local electron exchange interaction potential, and in some works also for spin-orbit interaction [40, 41, 42, 43, 44, 45].

A number of authors [46,47,33,32] suggested to use the quasi-classical approximation for calculations of dipole matrix elements. As it is shown in [publ1], the agreement with the more sophisticated full quantum-mechanical calculations for Rb, Na,

H (*n*S, *n*P, *n*D states) by Aymar [48] and quasi-classical approximation [33] are in the range of 10-20%.

For the line strengths calculations of the Na(3p-3s) transition, the ab inito methods have been used in nineties. To calculate the line strength, Guet et al. [49] used many-body perturbation theory (MBPT). To obtain the same quantity, Salomson at al [50] applied the coupled-cluster approach including single and double excitations (CCSD). The best agreement with the recent experimental results can be achieved using the multiconfiguration Hartree-Fock calculation with an approximate treatment of core-core polarization (MCHF-CCP) [51] and the large scale multiconfiguration Hartree-Fock and configuration interaction (MCHF –CI) calculation of Jönsson at al [52].

The reason we calculated the above mentioned quantities is that the optical excitation of Rydberg states and photoionization of atoms are often used in contemporary atomic physics experiments. Rydberg states in the molecular beam experiments involving Na atoms [11] are generated by laser excitation from the readily populated $3p_{3/2}$ state of Na. In accordance with the experimental needs like those in experiment [11], the following tasks have been set for this part of thesis work:

1) **To obtain Na $3p_{3/2} \leftarrow n s_{1/2}$, $n d_{5/2}$, $n d_{3/2}$ transition probabilities for principal quantum numbers up to n=50 and photoionization cross sections from Na(3p3/2) to continuum.**
2) **To test, with a variety of model potentials and parameter sets of these potentials, the accuracy of our calculations of transition probabilities and ionization cross sections, and to compare the obtained Na lifetimes, transition probabilities and photoionization cross sections with the available experimental and theoretical data. To show that a simple model potential method regarding electron-core penetration and the local electron exchange interaction give reliable excitation and ionization cross sections with the accuracy of 5%.**

2.2. Model potential

Dipole transition probabilities between the initial $n_0 l_0 j$ and final nlj atomic states are proportional to square of the dipole transition matrix element $\left|\left\langle n_0 l_0 j_0 \| D(r) \| nlj \right\rangle\right|^2$. To calculate these matrix elements, we need to know wavefunctions of the initial and final atomic states. In our study, the wavefunctions were calculated using Schrödinger equation with one-electron model potential method described bellow.

The one-electron model potential method assumes that the valence electron of the Na atom moves in the potential of core electrons and the nucleus. Using the one-electron model potential, the Schrödinger equation in atomic units is

$$\left(-\frac{1}{2}\nabla^2 + V(r)\right)\Phi_{nlm} = E_{nlm}\Phi_{nlm}, \tag{28}$$

where $V(r)$ is the potential for the valence electron and E_{nlm} denotes the eigenvalues. The wavefunctions Φ_{nlm} can be separated in radial $P_{nl}(r)$ and angular $Y_{lm}(\theta,\varphi)$ parts:

$$\Phi_{nlm}(r,\theta,\varphi) = \frac{1}{r}P_{nl}(r)Y_{lm}(\theta,\varphi).$$

Equation (28) for the radial functions $P_{nl}(r)$ was is integrated numerically using the Numerov method [53]. The potential $V(r)$ consists of three terms:

$$V(r) = V_c(r) + V_{cp}(r) + V_{exch}(r), \tag{29}$$

where $V_c(r)$ is the coulomb potential of unperturbed Na^+ ion, $V_{cp}(r)$ is the part of the total potential related to the core polarization, and $V_{exch}(r)$ is the exchange potential. The coulomb potential $V_c(r)$ was determined from the Hartree-Fock (HF) calculation of Na^+ radial charge density distribution. It has been brought into the following analytical form:

$$V_c(r) = -\frac{1}{r} - \frac{10}{r}\left((1+C_0)e^{-\eta_4 r} - C_0 e^{-\eta_3 r}\right) + \sum_{i=1}^{2} e^{-\eta_i r}\sum_{k=0}^{2} C_{ki} r^k . \tag{30}$$

The fitting parameters C_0, C_{ki} and η_i were obtained in [publ5]. For the Na^+ ion the numerical values of these parameters are given in table 1.

C_{01}= -8.7378391	C_{11}= -80.399335	C_{21}= -161.543600
C_{02}= -50.416327	C_{12} = 17.6504939	C_{22}= -21.2109560
C_0 = -0.732368	η_1 = 33.56251	η_2 = 4.8411970
η_3 = 11.201713	η_4 = 4.6234710	

Table 1. Parameters of the coulomb potential $V_c(r)$

The second term in eq. (29), $V_{cp}(r)$, is a correction term that accounts for polarization of the core electron cloud by the valence electron, i.e., it takes into account changes in the Na^+ charge distribution induced by the valence electron. The iterative perturbation procedure described by Bottcher [54] has been employed to obtain a semi-empirical model potentials of the form [40]:

$$V_{cp}(r) = -\frac{\alpha_d}{2r^4}\left[1-\exp\left(-\frac{r}{r_c}\right)^6\right] - \frac{\lambda}{2r^6}\left[1-\exp\left(-\frac{r}{r_c}\right)^8\right] \qquad (31)$$

Here α_d is the static dipole polarizability of the core. For Na^+, α_d=0.9947, r_c =1.00, λ=6.9273. Outside the core distribution, this potential behaves like $-1/r^4$ due to the induced dipole and like $-1/r^6$ due to the induced quadrupole and the dynamic polarizability. The divergence disappears for a core of finite size and is usually handled by a cut-off function. This form was used by Weisheit [40] to calculate the ground-state photoionization cross sections and oscillator strengths for Na, Rb, Cs, K, and later for alkali lifetime calculations by Theodosiou [44]. The cut-off radius r_c is usually chosen by matching the calculated and measured energies of the outer electron. For l = 0, 1, the values of r_c turn out to be close to the values recommended in ref. [40]. An alternative form of the core polarization potential is [55]:

$$V_{cp}(r) = -\frac{\alpha_d}{2r^4}\left[1-\exp\left(-\frac{r}{r_c}\right)^2\right]^2 . \qquad (31a)$$

The potentials (31) and (31a) differ mainly at small radii. For r/r_c<<1, the potential (31) approaches zero, whereas (31a) turns to a constant value.

In paper [56] an ab inito approach to construct appropriate core polarization potentials using configuration interaction Pauli-Fock (CIPF) calculations is described, which incorporates relativistic and many electron effects. Numerical core polarization

potential has been derived in [56] applying variation principle for the total energy of the atom written with the second order correlational corrections.

The third term of eq. (29) is accounting for the local electron exchange potential [54, 40], and it can be expressed as

$$V_{exch}(r) = (c_0 + c_1 r)\exp\left(-\frac{r}{r_c}\right).$$

The parameters r_c, c_0, and c_1 are chosen such as to adjust the individual eigenvalues of eq. (28) to the corresponding experimental energy value given in [57]. In our study we used the following numerical values of these parameters given in ref [40]: c_0=0.38514, c_1=-0.10506.

2.3. Transition probabilities and transition dipole moments

The transition probability for spontaneous emission in atomic units is [58]:

$$A(n_0 l_0 j_0 \to nlj) = \frac{4}{3(2j_0+1)}\alpha^3(\Delta E)^3\left|\langle n_0 l_0 j_0 \| D(r) \| nlj\rangle\right|^2, \qquad (32)$$

where α is the fine structure constant and the transition energy is $\Delta E = E_0 - E$. The dipole matrix element can be written as:

$$\left|\langle n_0 l_0 j_0 \| D(r) \| nlj\rangle\right|^2 = (2j_0+1)(2j+1)\begin{Bmatrix} l_0 & j_0 & 1/2 \\ j & l & 1 \end{Bmatrix}^2 \max(l_0, l) R(n_0 l_0 j_0; nlj)^2 \qquad (33)$$

The 6-*j*-symbol $\begin{Bmatrix} * & * & * \\ * & * & * \end{Bmatrix}$ accounts for the result of integration over angular coordinates.

To determine the transition probability it is necessary to calculate the radial transition dipole moment

$$R(n_0 l_0 j_0; nlj) = \int_0^\infty dr P_{nlj}(r) D(r) P_{n_0 l_0 j_0}(r). \qquad (34)$$

The central task here is to determine the radial wavefunctions $P_{njl}(r)$ from the radial Schrödinger equation.

In zero-order approximation the dipole moment operator is $D^{(0)}(r)=r$. To calculate the transition probability more precisely, one has to account for the core polarization. The dipole moment operator for the potential (31) then becomes [59, 40]:

$$D^{(1)}(r) = r\left\{1 - \frac{\alpha_d}{r^3}\left[1 - \exp\left(-\frac{r}{r_c}\right)^3\right]\right\}, \tag{35}$$

and for the potential (31a) [55]:

$$D^{(1)}(r) = r\left\{1 - \frac{\alpha_d}{r^3}\left[1 - \exp\left(-\frac{r}{r_c}\right)^2\right]\right\}. \tag{35a}$$

The transition dipole moments calculated with dipole moment operators $D^{(0)}(r)$ and $D^{(1)}(r)$ differ from each other by ca 2%.

In order to deal with high values of n, it is useful to remember that, according to quantum-defect theory, for sufficiently large n the energy of the Rydberg states may be expressed in terms of quantum defects μ_l as

$$\varepsilon = -\frac{1}{2}(n - \mu_l)^{-2}.$$

With this relation, an energy-normalised transition moment can be defined for $\varepsilon < 0$ as

$$R_\varepsilon^2(n_0 l_0 j_0; \varepsilon l j) = R^2(n_0 l_0 j_0; n l j)\left(d\varepsilon / dn\right)^{-1} = R^2(n_0 l_0 j_0; n l j)(-2\varepsilon)^{-3/2}$$

This energy-normalised transition moment connects smoothly with the continuum transition moment function. The calculated transition moments of Na($3p_{3/2}$) for Rydberg and continuum states with potential (31) and operator (35) are cast by least squares fitting into the analytical expression:

$$R_\varepsilon \approx \sum_{i=1}^{3} A_i \exp(-\varepsilon\alpha_i) \qquad -0.014 \le \varepsilon \le 0.07 \text{ (a.u)} \tag{35}$$

with parameters A_i and α_i as given in table 2. The transition moments are shown in fig. 8. Calculated transition probabilities for spontaneous emission with formula (32) from levels with $n \le 50$ to the Na($3p_{3/2}$) state are given in [publ5], together with other theoretical values for the lowest transitions.

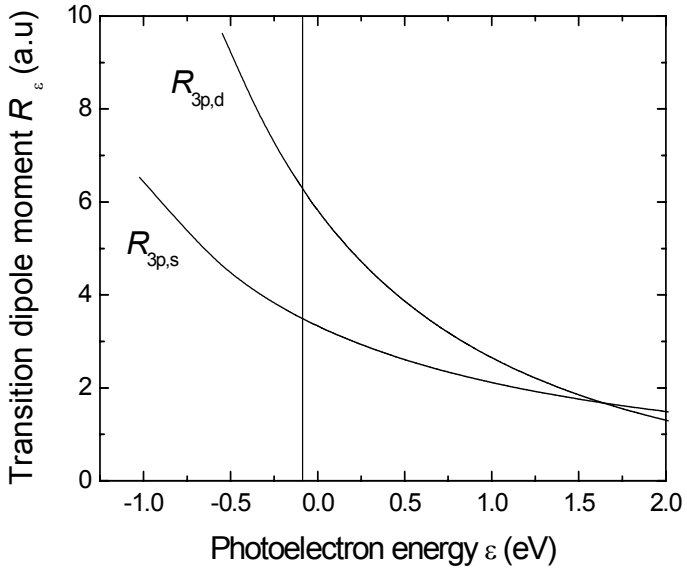

Fig. 8. Transition dipole moments of Na($3p_{3/2}$) for Rydberg and continuum states. The vertical line separates the region where discrete moments are calculated from bound states from the region where the continuum formula is used.

	$3p_{3/2} \rightarrow \varepsilon$ d				$3p_{3/2} \rightarrow \varepsilon$ s		
A_1	5.02081	α_1	18.4638	A_1	2.25476	α_1	6.7440
A_2	0.80447	α_2	55.7103	A_2	1.06396	α_2	29.8329
A_3	-0.00026	α_3	370.3704	A_3	0.01312	α_3	88.2613

Table 2: Parameters for transition dipole moments of Na($3p_{3/2}$), eq. (36).

2.4. Photoionization cross sections

In this thesis [publ5] we applied the approach described above to study theoretically process of photoionization for the reaction $Na(3p_{3/2}) + \gamma \rightarrow Na^+ + e^-(\varepsilon s, \varepsilon d)$. In this process the valence electron of sodium atom absorbs a photon with energy, which exceeds the photoionization threshold energy of 3.029 (eV) by photoelectron energy $\varepsilon > 0$. As the result, a sodium ion and a photoelectron with energy ε are formed. The total photoionization cross section is a sum of partial cross sections of photoionization from ($l_0=1$, $j_0=3/2$) into s states ($l=0$, $j=1/2$) and d states ($l=2$, $j=3/2$, $5/2$) [58]:

$$\sigma_{j_0}(\Delta E)[\mathrm{Mb}] = \frac{4}{3}\pi^2 \alpha a_0^2 \Delta E \frac{1}{2j_0+1}\sum_{lj}\left|\left\langle n_0 l_0 j_0 \| D(r) \| \varepsilon l j \right\rangle\right|^2 ,$$

where $\Delta E=\varepsilon-E(3p_{3/2})$ is the exciting photon energy in atomic units and a_0^2 is squared Bohr radius. The transition dipole operator $D(r)$ can be taken as (35) or (35a). The radial part of the transition dipole moment $R_\varepsilon(n_0 l_0 j_0;\varepsilon,l,j)$ is defined by eq. (34), and it can be calculated with energy-normalized continuum wavefunction.

Fig. 9 shows the photoionization cross sections for $Na(3p_{3/2})$ as a plot of electron energy obtained using semi-empirical model potentials of the form (31). For comparison, the cross sections obtained in earlier theoretical and experimental studies [60, 61, 43, 62, 63, 64] are shown. The most cited theoretical works from seventies among them, [64] and [42], used a semi-empirical model potential. In those studies, the optimal potential parameters were determined by minimizing the root-mean-square deviation between observed and calculated energies of selected levels. The photoionization cross sections calculated in our study agree with those of [42] within the graphical scanning uncertainty because the photoionization cross sections are only available in graphical representation. Therefore they are not separately shown in fig. 9. The calculation of [64] differs from the present results by ca 5 - 7 % (see fig. 9). In our study, the parameter set of the model potential of the initial state was obtained according to the experimental value of the energy of the $3p_{3/2}$ state given in [57]. For the potentials of continuum states the parameters were obtained by energy matching for states with n>15. The agreement between our photoionization cross sections and the cross sections obtained by the configuration interaction Pauli-Fock calculation with core potential approximation [63] is less satisfactory. The photoionization cross sections of [63] are by 8% higher than those of the present work.

The first experimental determination of the photoionization cross sections was based on electron–ion recombination data and has been reported in [60]. Photoionization cross sections obtained in the present study agree with the experimental results of [60] within 1 % near the ionization threshold, but difference increases up to 10-15%, when photoelectron energy increases above 1 eV. In the sodium beam experiment [43], the partial photoionization cross sections $\sigma_{3p\to s}$ and $\sigma_{3p\to d}$ to the continuum s and d states were measured separately using two appropriately polarised light sources. These

measurements were done over the photoelectron energy range $0 \le \varepsilon \le 0.37$ eV with an estimated accuracy of 5-10%. The results of the present calculation agree within 5% with the latter experiment. In [62], the photoionization cross sections were measured using monochromatised synchrotron radiation ionising Na($3p_{3/2}$) over the range $0 \le \varepsilon \le 2.1$ eV with an estimated accuracy of 25%. The curve representing these data is considerably steeper than curve obtained in our studie (see fig 9.). At $\varepsilon > 1.6$ eV the curve of [62] exhibits an increase in the cross section. This is due to photoionization of the 3s electrons of ground-state Na atoms.

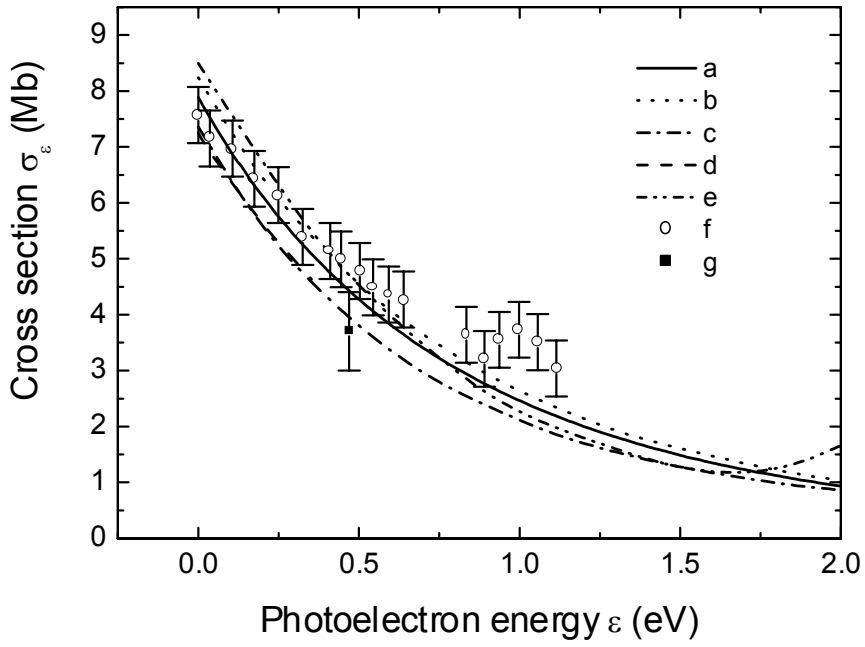

Fig. 9. Photoionization cross-sections σ(ε) for the Na($3p_{3/2}$) atom over the photoelectron energy range 0-2.0 eV. [a]: Hartree Fock calculation with semi-empirical core polarization potential and local exchange potential (Publ5); [b]: configuration interaction tecnique with Pauli-Fock atomic orbitals and core polarization potential [63]; [c]: Parametric central potential [64]; [d]: laser ionization experiment [43]; [e]: ionization with monochromatized synchotron radiation [62]; [f]: cross-sections from electron-ion recombination data [60]; [g]: saturated ionization with pulsed laser [61];

2.5. Conclusion

In this thesis, probabilities for phototransition of Na($3p_{3/2}$) atoms have been calculated using the model potential method with local potential approximation in the form (31, 31a). Parameters of the model potentials were adjusted to reproduce

experimental energy eigenvalues [57]. From tests with a variety of parameter sets we estimate that the resulting transition probabilities to lower excited states vary in comparision with reliable experimental and theoretical data in the range of 2-3%. This accuracy is also assumed for the photoionization cross sections for ε<0.5 eV. Relative uncertainty may grow ε>0.5 eV up to 4-6% due the decrease of photoionization cross sections at higher energies. The calculated Na $3p_{3/2} \leftarrow n s_{1/2}$, $n d_{5/2,}$ $n d_{3/2}$ transition probabilities are tabulated up to n=50 and lifetimes are compared with available experimental data. Earlier calculations with energy-adjusted model potentials are validated. The photoionization cross sections from the $3p_{3/2}$ state are presented in the form of an analytical formula. The results obtained using the quasi-classical approximation were of poorer accuracy 20-30% as compared to the model potential method. We can conclude that the model potential method is useful for obtaining reliable theoretical data.

3. Semiclassical treatment of radiation trapping in spatially nonuniform media

3.1. Introduction.

If a gas consist of many atoms of the same kind, then a photon emitted by an atom within such optically thick medium will be absorbed and reemitted repeatedly by other atoms before it will escape from the medium. This process is know as radiation trapping [65]. Radiation traping plays an important role in various physical processes. As an example radiative energy transfer in planet atmospheres can be mentioned. Radiation trapping in an atomic vapour can influence many spectroscopic experiments. Radiation trapping is described by the rate equation for the excited-state atom density in the vapour cell called Biberman-Holstein equation (eq. 37) [9]. The overview of various methods allowing the solution of Biberman-Holstein equation can be found in [9]. All traditional methods, which find analytical solutions of radiation trapping equations, deal with simple model situations as one-dimensional geometries, spatially uniform media, high optical thicknesses and so on. The best of numerical methods, which can be used to solve the trapping equations for arbitrary cell geometries, is the numerical Monte-Carlo method [66]. Implementation of this method is computationally demanding. It requires powerful computers and long computation times particularly at high opacity. The authors of paper [67] introduced new method called the geometric quantization technique (GQT). This is a general analytical approach for solving the Biberman-Holstein equation. GQT was applied to the solution of one-dimensional [67], and two- and three-dimensional problems [10]. Efficiency and advantages of this method become more pronounced, when more complex problems are considered, for example radiation trapping in elliptical cells.

Task of this work was to prove the applicability of GQT method in more complicated geometries, like elliptical cylinders, and prolate and oblate ellipsoids. The method also had to be compared with numerical Monte-Carlo calculations. Finally, ready-to-use recipes for computation of the radiation trapping factors in elliptical cells had to be provided.

3.2. Biberman-Holstein equation

An atom in a dense vapour may be excited by externally applied radiation plus the fluorescence from other excited atoms within the vapour, and it will decay by spontaneous emission. This is expressed by the Holstein–Biberman equation for excited-state atom density $n^*(\vec{r},t)$:

$$\frac{dn^*(\vec{r},t)}{dt} = S(\vec{r},t) - [A_{21} + W(\vec{r})]n^*(\vec{r},t) + A_{21}\int_{\Omega} d^3\vec{r}\,' G(|\vec{r}-\vec{r}\,'|)n^*(\vec{r},t) \quad (37)$$

$$G(\rho)G = -\frac{1}{4\pi\rho^2}\frac{\partial T(\rho)}{\partial \rho} \quad (38)$$

$$T(\rho) = C_n \int_{-\infty}^{\infty} k(v)exp(-k_0\rho k(v))dv \quad (39)$$

$$\rho = |\vec{r}-\vec{r}\,'|$$

Here Ω is the gas volume, confined atomic vapour. $S(\vec{r},t)$ is the excitation rate due to externally applied radiation, A_{21} - Einstein coefficients for spontaneous decay, W – non-radiative quenching rate, $G(|\vec{r}-\vec{r}\,'|)$ - probability that a photon that is emitted at point $\vec{r}\,'$ is absorbed at point $\vec{r}$, after it has travelled the distance $\vec{\rho} = \vec{r} - \vec{r}\,'$. The function G depends on the spectral profiles of absorption (Lorentz, Doppler or Voigt cases). $T(\rho)$ is the probability that a photon will pass distance ρ without absorption, and C_n is the normalization constant:

$$C_n = 1\Big/\int_{-\infty}^{\infty} k(v)dv \ . \quad (40)$$

The Biberman-Holstein equation assumes following assumptions:

1. We deal with a two-level atom.
2. The density of ground state atoms is assumed to be much larger than the excited-state density. It means that we may neglect the change of the ground-state density profile during radiation transport and the effects of stimulated emission from the upper level.
3. There is no photon reflection at the cell surface; every photon which reaches the cell surface escapes or is fully absorbed. When this condition is violated, we should

change the kernel function of radiation transport to include the effect of photons reflected at the wall.

4. Neglect the flight time of photons. This assumption is acceptable in any nonrelativistic system.
5. Spatial diffusion of atoms is negligible
6. The frequency of a re-emitted photon is assumed to be completely independent of that of the absorbed photon. This is called complete frequency redistribution. Frequency distribution of the reemision $\varphi(\nu)$ and absorption $k(\nu)$ profiles are proportional to each other: $\varphi(\nu)= C_n k(\nu)$

We consider a given initial spatial distribution at the time t=0. At times t>0 no external excitation (i.e., radiation) sources are presented ($S(\vec{r},t)=0$). Fourier solutions to Eq. (37) are of the form:

$$n^*(\vec{r},t)=\sum_j \alpha_j \psi_j(\vec{r}) exp(-A_{21}t/g_j) \tag{41}$$

where $\psi_j(\vec{r})$ are the normalized eigenmodes, $\lambda_j=\frac{1}{g_j}$ are the corresponding eigenvalues of the Biberman-Holstein equation (37), α_j are expansion coefficients of the initial distribution of excited state population over eigenmodes. Parameters called trapping factors g_j give the number of reemission processes that a photon in the jth mode undergoes before leaving the cell. The effective lifetime of the fundamental mode is:

$$\tau_0=\frac{g_0}{A_{21}}, \tag{42}$$

Lifetime of the jth mode decreases with increasing mode number ($\tau_0 > \tau_1 > \tau_2 > \tau_3 >$.....). Therefore, the solution of the equation (37) can be qualitatvely characterized using the fundamental mode. Hence, the first task to find the trapping factor g_0, i.e., the lifetime of the fundamental mode τ_0.

3.3. Geometric Quantization Technique

The main difficulty in analytical treatment of eq. (37) arises due to presence of far-wing photons, and they exist in all practically occurring line shapes. The far-wing photons are those with frequencies corresponding to the wings of the given absorption $k(\nu)$ profile. Because of these photons, the mean free path of spacial diffusion of photons becomes infinite [9], such that many conventional numerical calculation schemes become inadequate. On the other hand, the more universal Monte Carlo method requires long computation times. Therefore it is of interest to develop simple and sufficiently universal analytical approaches.

In present work we propose a novel GQT approache [67], which allows us to find the eigenfunctions of eq. (37). One can write the Biberman-Holstein equation (37) in the form:

$$\frac{dn^*(\vec{r},t)}{dt} = A_{21}(\hat{I}-\hat{G})n^*(\vec{r},t) + W(\vec{r})n^*(\vec{r},t), \tag{43}$$

where symbol $\hat{G}$ denotes the integral operator of $G(\rho)$ in eq. (37) and $\hat{I}$ is the identity operator. The eigenfunctions $\psi_j(\vec{r})$ of eq. (43) can be found by solving it together with eq. (41). It can be show that $\psi_j(\vec{r})$ obeys the following equation:

$$A_{21}\lambda_j\psi_j(\vec{r}) = A_{21}(\hat{I}-\hat{G})\psi_j(\vec{r}) + W(\vec{r})\psi_j(\vec{r}). \tag{44}$$

The main idea in the application of GQT to radiation trapping is to write the trapping equation (44) in the same form as a steady-state wave equation for some "quasiparticle" [67]. This steady-state wave equation contains the following Hamiltonian H associated with eq. (44) [66]:

$$H(\vec{p},\vec{r}) = A_{21}\widetilde{V}(\vec{p}) + W(\vec{r}), \tag{45}$$

where

$$\widetilde{V}(\vec{p}) = 1 - \int_{-\infty}^{\infty} d^3r \exp(i\vec{r}\cdot\vec{p})G(\vec{r}). \tag{46}$$

For a gas contained in an infinite space $\Omega=\Omega_\infty$ under the conditions when there is no quenching (i.e., W=0), the eigenfunctions of operator $\hat{I}-\hat{G}$ are planar waves $\exp(i\vec{r}\cdot\vec{p})$.

$$(\hat{I}-\hat{G})\exp(i\vec{r}\cdot\vec{p})=\int_{-\infty}^{\infty}d^3r'\exp(i\vec{r}'\cdot\vec{p})[\delta^3(\vec{r}-\vec{r}')-G(\vec{r}-\vec{r}')]=\tilde{V}(\vec{p})\exp(i\vec{r}\cdot\vec{p}).$$

These planar waves with the wave vector $\vec{p}$ describe the waves associated with a free quasi-particle. The corresponding eigenvalues $\lambda_p=\tilde{V}(\vec{p})$ are obtained by Fourier transform of the kernel function δ^3-G, where δ^3 is the Dirac's δ function. Using the system of units with $\hbar$=1, one can interpret the wave vector $\vec{p}(cm^{-1})$ as the momentum of quasi-particle, while the trapping rate constant (i.e., inverted lifetime) is interpreted as its kinetic energy:

$$\tau^{-1}=A_{21}\tilde{V}(\vec{p}). \qquad (47)$$

The quenching rate $W(\vec{r})$ can be interpreted as the potential energy of the quasiparticle [68, 69]. From the wave-particle dualism we can conclude that equation (44) describes a quasi-particle associated with the Hamiltonian H (45), which is imprisoned in the vapour cell of the shape described by Ω. The absence of atoms outside the cell means that there is an infinite potential jump $\Delta W=\infty$ at the cell surface. In addition we assume that there is no photon reflection at the cell surface. This implies a boundary condition that the quasi-particle is elastically reflected from surface $\partial\Omega$ confining the volume Ω of the absorbing medium. If the quenching within the absorbing volume Ω can be neglected (i.e., W=0), then the problem of finding the trapping factors g_j reduces to the determination of the quantized energy spectrum of quasi-particle with the Hamiltonian $H(\vec{p},\vec{r})=A_{21}\tilde{V}(\vec{p})$. In order to solve this problem, we involve additional modifications of the semiclassical approach, which are known also as the "short–wavelength approximation'' in optics. In this approximation we deal with a typical quantum billiard-like problem and consider of the quasiparticle trajectories as straight lines (fig. 10). Using the Fourier transform for kernel δ^3-G the kinetic energy $A_{21}\tilde{V}(\vec{p})$ of the quasi-particle can be expressed by spectral absoption coefficients of the given atomic transition [70]:

$$\widetilde{V}(\vec{p}) = 1 - \frac{1}{|\vec{p}|}\int_{-\infty}^{\infty} C_n k_0 k(v)^2 \arctan\left(\frac{|\vec{p}|}{k_0 k(v)}\right) dv \qquad (48)$$

As can be seen, $V(\vec{p})$ is subject to a rather complicated dispersion law, which leads to generation of photons at frequencies corresponding to far wings of the spectral line profiles.

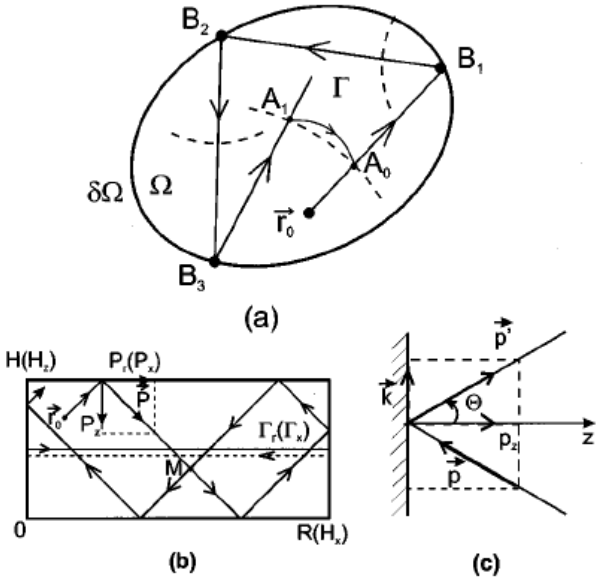

Fig. 10. Illustration of the multidimensional quantization rules. The dashed lines in (a) give the wave-fronts produced by reflections from the boundary of the absorbing medium. The billiard-like trajectory in (b) appears for radial motion of the quasi-particle in a finite cylinder or in a 2D rectangular box. In (c), the reflection of quasi-particle reflection from a plane potential wall is shown.

3.4. Quantisation Rules

The quasiparticle moves along a classical trajectory $\{\vec{p}(t), \vec{r}(t)\}$. If quenching is negligible (W=0), then the motion equation can be written as:

$$\vec{\upsilon} \equiv \frac{d\vec{r}}{dt} = \frac{\partial H}{\partial \vec{p}} = \frac{\partial \widetilde{V}}{\partial \vec{p}} = const\,, \quad \frac{d\vec{p}}{dt} = -\frac{\partial H}{\partial \vec{r}} = -\frac{\partial \widetilde{V}}{\partial \vec{r}} = 0\,.$$

According to the above equations, the quasiparticle travels along a straight line equations and condition (W=0) quasiparticle travels along a straight line ($\vec{p}$=const) within the volume Ω, until it reaches the boundary ∂Ω. From this boundary the quasi-particle is elastically reflected back into the volume Ω and continues motion along a straight path (see fig. 10). The dotted lines in fig. 10.a represents sections of wave-front surfaces associated with the semiclassical wave function of the quasiparticle. After several

reflections, the initial wave-front transforms into itself (point A_1 in fig 10.a). From the semi-classical point of view, the search for the solutions of wave equation (44) with the Hamiltonian H (45) is equivalent to defining resonance conditions for the quasiparticle. In other words, solution of the problem is equivalent to finding standing-wave solutions for the wavefunction. We can now apply Bohr–Sommerfeld semiclassical quantization rules [71]. It implies that phase change of the wave along arbitrary closed path Γ_r must be an integer multiplie of 2π:

$$2\pi I_r - \sum_{(r)} \Delta S_i = 2\pi j_r , \qquad I_r \equiv \frac{1}{2\pi} \oint_{\Gamma_r} \vec{p}(r) d\vec{r} , \quad j_r=0,1,2\ldots \tag{49}$$

The above equations mean that the wave front evolves until it recovers its initial position. The path Γ corresponds to the trajectory: $\Gamma=A_0 B_1 \cup B_1B_2 \cup B_2 B_3 \cup B_3A_1 \cup A_1A_0$ (see fig. 10.a). Boundaries $\partial\Omega$ are associated with repulsive potential energy, which leads to phase jumps ΔS_i along Γ_r that must be taken into account. The resonance condition (49) for an arbitrary closed path can be reduced to finite number m of equations (49). These correspond to for m topology-independent cycles, where m is the dimension of the cell $j=\{j_1 \ldots j_m\}$. For a 3-dimensional gass cell m=3 (e.g., sphere, ellipsoid, cylinder, parallelepiped and all other 3D vapour cell geometries). From the quantisation rules (49) one can calculate the momentum $\vec{p}^{(j)}$ of the wave mode $\psi_j(\vec{r})$, from which, in turn, the kinetic energy $A_{21}\widetilde{V}(\vec{p}^{(j)})$ of the quasiparticle can be determined using eq. (48). Eigenvalues λ_j and trapping factors g_j can then be found as:

$$\frac{1}{g_j} = \lambda_j = \widetilde{V}(p^{(j)}) \tag{50}$$

3.5. Boundary phase jumps of the quasiparticle

The infinite potential jump $\Delta W=\infty$ at the vapour cell surface $\partial\Omega$ causes phase jump ΔS in the de Broglie wave of the quasi-particle, which is reflected from the wall. This phase jump can be written as

$$\Delta S(p_z, |\vec{k}|) = \frac{\pi}{2} - \frac{2}{\pi} \int_0^1 ln\left(\frac{\widetilde{V}_k(p_z) - \widetilde{V}_k(p_z\rho)}{\widetilde{V}_k(p_z/\rho) - \widetilde{V}_k(p_z)} \right) \frac{1}{1-\rho^2} d\rho , \tag{51}$$

$$\widetilde{V}_k(\eta) = \widetilde{V}\left(\sqrt{\eta^2 + p^2 sin^2(\theta)}\right), \qquad p_z = pcos\theta$$

The value of phase jump ΔS depends on the angle θ, at which the wave is reflected (fig. 10.c). The above equation was derived for the half-space in [67] (e.g., the coordinate space with $z \geq 0$ or $z \leq 0$ and infinite planar potential wall at z=0). We can use this result also for other geometries. For the half-space $z \geq 0$ (fig. 10.c), eq. (44) describes eigenfunction $\Psi_p(z)$ for a quasiparticle with the momentum $\vec{p}$. This eigenfunction consists of the incoming wave, exp(-$ip_z z$), and the reflected wave, exp($ip_z z$-$i\Delta S$). In other words, the asymptotic behavior (z>>0) of the solution of eq. (44) can be found in the form of a standing wave:

$$\Psi_p(z) \approx C[exp(-ip_z z) + exp(ip_z z - i\Delta S)] = \widetilde{C}\, cos(p_z z - \Delta S/2), \qquad (52)$$

where the phase jump ΔS is the same as in eq. (51). The layer, within which the 'interaction' between the quasi-particle and the boundary of the medium must be taken into account (from physical point of view, this layer corresponds to some transition zone, where the proceeses of photon escaping from the vapour cell are compensated by the photons outgoing from the cell optically deep layers), is given by the interaction length ΔL_{int} [10]:

$$\Delta L_{\text{int}} \approx \frac{\sin(\Delta S)}{2p} + \frac{1}{2}\frac{d(\Delta S)}{dp}$$

Hence, the interaction length defines the layer adjacent to the potential wall (i.e., the cell boundary), in which the formation of the standing wave takes place, so that for z>ΔL_{int} the quasiparticle may be considered as a free particle and eq. (52) can be employed. The interaction length increases when the quasi-particle moves along the potential wall. If $p_z < |\vec{p}|$, then the length of the path of quasi-particle through the boundary zone ΔL_{int} is $\left(|\vec{p}| \big/ p_z\right)\Delta L_{\text{int}}$. For the reflection angle θ=π/2, the value of $\frac{|\vec{p}|}{p_z} \to \infty$, i.e., the motion of quasi-particle is confined within the boundary zone. In that case, the phase jump becomes maximal: $\Delta S_{max} = \pi$.

For the quantization rules to be valid, the lenght ΔL_{int} must be smaller than the characteristic distance between two reflections : $\Delta L_{int}<L$, where L is the geometrical size of the cell. The value of ΔL_{int} is the largest for the fundamental mode [10]. The phase jump (51) depends from the absorption coefficient k_0 and the absorption lineshape. From the quantum uncertainty relation pL=1 it follows that the non-dimensional ratio $k_0/p= k_0L$ corresponds to opacity of the vapour cell k_0L.

If the cell is elliptical, then the quasi-particle is reflected from the vapour cell walls at different angles, which leads to different phase jumps ΔS. This situation is considered in [10] using the Percival semiclassical variation method in determining the quasiparticle trajectory. It is shown [10] that ΔS must be averaged along the reflecting boundary $\partial\Omega$. In elliptical coordinates (η, ξ) averaging of ΔS along the surface $\partial\Omega(\eta = \overline{\eta})$ leads to the mean phase jump value:

$$\left\langle \Delta S_{\eta=\overline{\eta}} \right\rangle = \frac{\int\limits_{\eta=\overline{\eta}} \frac{d\xi}{p_\xi} \Delta S_{\eta=\overline{\eta}}(\xi)}{\int\limits_{\eta=\overline{\eta}} \frac{d\xi}{p_\xi}} \qquad (53)$$

For various geometries (sphere, ellipsoid) an additional phase shift is possible due to other reasons of the semiclassical approach to be breaking down. It may be resulted, for instance, because of occuring the caustic surface for the quasi-particle trajectories. The caustics correspond to turning points of the motion of quasi-particle in the space of generalized spatial variables. Usually, those variables are determined via a set of trajectories, which are creating the new (generalized) coordinate lines. Actually, one need to proceed along the trajectory provided he works under generalized variables. The latter results in appearing of effective (centrifugal) additional potentials in the equation of motion of the quasiparticle. The caustics correspond to the situation when the quasiparticle is reflected from the effective potential barrier. The corresponding phase jump on the caustic is given by [80] :

$$\Delta S_{cau}=\pi/2 \qquad (54)$$

Note, that the above equation (54) ignores the barrier effect. The barrier effects can not be always neglected. For example, they generally must be taken into account in elliptical cell

geometries (see, for instance [21]) except for the fundamental mode, for which they vanish [10].

3.6. Parallelepiped with sides of length H_x H_y H_z

At first one must solve the eigenvalue problem (44) and find the trapping factors g_j entering Eq (41). In order to do so, we will use the Bohr-Sommerfeld quantization rules (49). Note, that we deal mainly with cell geometries allowing the separation of variables (integrable systems). It means that different spatial variables can be considered as independent. Let us consider some examples. Motion of a quasi-particle inside the 3D parallelepiped with sides of length H_x H_y H_z can be decomposed in three independent motions along each of the x,y,z coordinates. The integral in eq. (49) is calculated along closed cycles Γ_I, which are parallel to the coordinate axes. The cycle Γ_x is shown in (fig. 10.b). The phase jumps occures only on the parallelepiped surfaces, and they can be determined from eq (51). The quantization rules (49) lead to a nonlinear system of three equations:

$$2H_i p_i = 2\Delta S\left(p_i, \sqrt{p^2 - p_i^2}\right) + 2\pi j_i$$

$$p^2 = p_x^2 + p_y^2 + p_z^2,$$

$I=x,y,z$

The solution of this system yields the momentum field $\vec{p}_0^{\,i} = \{p_x, p_y, p_z\}$. When the momentum field is known trapping factors g_j can be found from eq. (50).

3.7. Examples of elliptical geometries

Let us consider the following types of ellipsoidal cavities with semi-axes $R_>$ and $R_<$:

$$\frac{x^2}{R_>^2} + \frac{y^2}{R_<^2} = 1; \qquad -\infty < z < \infty; \qquad \text{elliptical cylinder,}$$

$$\frac{x^2 + y^2}{R_<^2} + \frac{z^2}{R_>^2} = 1; \qquad \text{prolate ellipsoid.}$$

Like in the case of 3D parallelepiped, also in the elliptical cells it is possible to separate the spatial variables. For ellipsoid and elliptical cylinder it is convenient to use the elliptical coordinates. The first step is to apply the Bohr-Sommerfeld quantization rules (49) rewritten for the elliptical coordinate system. As mentioned above, in elliptical cells the reflection of the quasi-from the boundary occurs at different angles, which leads to different values of ΔS. Hence, the value ΔS must be averaged along the reflecting surface $\partial\Omega$. For calculations we used in eq. (49) the average phase jump given by eq. (53), and the phase jump on the caustic given by eq. (54). Our computation of the trapping factors g_j is based on an iterative procedure. A practical recipe for calculation of the trapping factors g_j can be found in ref. [10]. Fig. 11 and 12 show the g_0 factors for the fundamental mode calculated using GQT for the case of a prolate ellipsoidal cell filled with a homogeneous absorbing medium.

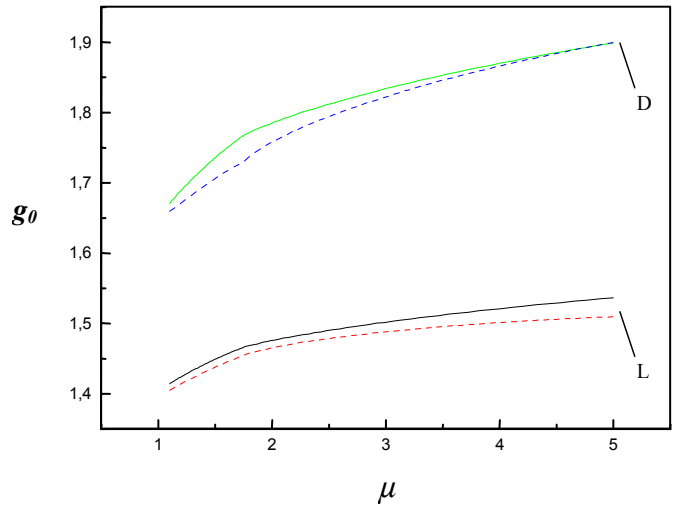

Fig. 11. Trapping factors g_0 for the fundamental mode for a prolate ellipsoid at the opacity $k_0L = k_0R_<=1$. The values of g_0 obtained by GQT (solid lines) are shown as a function of the semi-axes ratio $\mu=R_>/R_<$. Dashed lines show the results of numerical calculations by Monte Carlo method. The calculation have been performed for Lorentz and Doppler spectral line profiles.

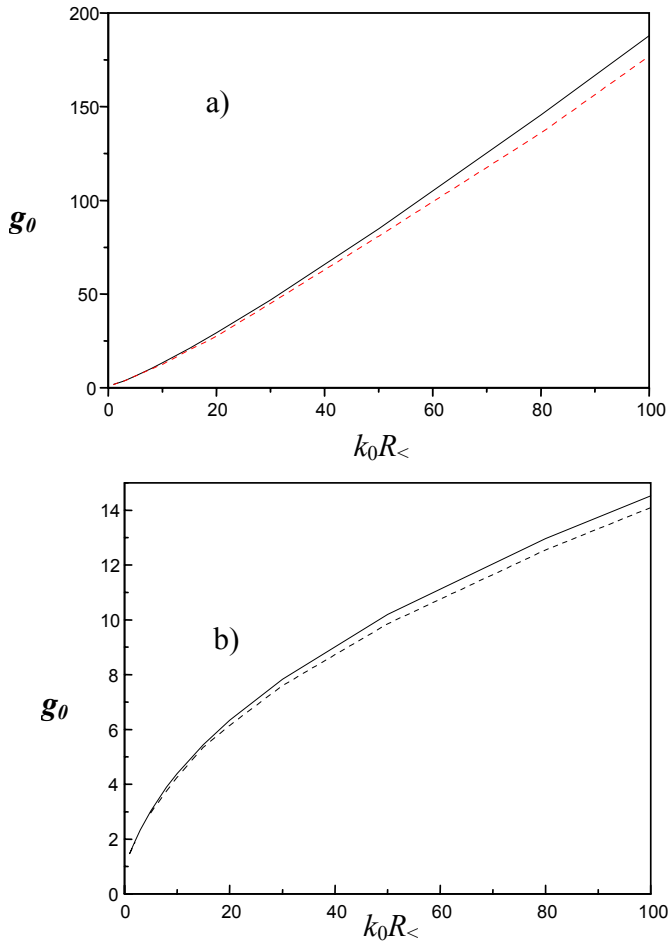

Fig. 12. Trapping factor g_0 for a prolate ellipsoid as a function of vapour cell opacity $k_0L= k_0 R_<$ for the fundamental mode. (a) and (b) represent calculations for Doppler and Lorenz lineshapes, respectively. The solid and dashed lines corresppond to results obtained by GQT and Monte Carlo methods, respectively. The semi-axes ratio is fixed to $\mu=R_>/R_< =2$.

As one can see, the results of GQT calculations for prolate ellipsoid agree with the results of Monte Carlo calculations to within a 5% difference in the case of fundamental mode. Agreement between both calculations is somewhat poorer in the case of oblate ellipsoid, but it is still better than 10%. For all higher order modes the accuracy of the determination of trapping factors g_j by GQT is better than 0.5%. Since we find a good agreement between the Monte Carlo and GQT calculations in the case of elliptical cell geometries, it is reasonable to assume that the average phase jump given by eq. (53) is valid for cells with more complicated geometries.

3.8. Conclusion

We have demonstrated that GQT is a useful instrument allowing the solution of classical radiation trapping problems. GQT provides analytical description for various geometries of the absorbing media. The results obtained by GQT were compared with the results of Monte-Carlo calculations. From this comparison we conclude that the accuracy of the calculation of the trapping factor of the fundamental mode, g_0 , is about 5%, while for higher modes it is better than 0.5%. The advantage of the GQT method is obvious: the run time of Monte Carlo simulations quickly increases and becomes prohibitive as the opacities increased. In contrast GQT requires only very small numerical efforts. The second important advantage of GQT is that it allows a simple and efficient treatment of radiation trapping in geometries, which are unaccessible to other analytical and semi-analytical methods. In present work, we have shown that GQT can be successfully applied to radiation trapping problems in 2*D* and 3*D* vapour cells [10, 67, publ6]. We have also provided the formulation and solutions of radiation trapping problem in elliptical geometries of the absorbing medium, which are generally more complicated, because the reflection angle of the qusi-particle varies strongly with the position of the reflection point on the cell surface.

4. Photodissociation of Na_2 molecules

4.1. Introduction

Photodissociation process is an elementary chemical reaction of type:

$$AB + h\nu \rightarrow AB^* \rightarrow A + B^* \qquad (55)$$

In the photodissociation, a photon with frequency ν excites the molecule *AB* to a continuum state *AB**, from where it dissociates into two separate fragments *A* and *B**. Within the framework of Born-Oppenheimer approximation, the theoretical description of the direct photodissociation processes assumes that the electronic state excited by photon absorption is described by a potential energy surface, which is repulsive along the dissociation coordinate. This situation is represented in fig. 13. for the dissociation of a diatomic molecule. The strength of an electronic transition corresponding to the absorption of a photon is proportional to [8]:

$$\left| \int dR\, \chi_g(R)\, \mu_{gd}(R)\, \chi_d(R) \right|^2 , \qquad (56)$$

where χ_g and χ_d are the vibrational eigenfunctions of the initial (bound) and final (dissociative) states, respectively, and μ_{gd} is the matrix element of the electronic dipole moment operator for the electronic transition $g \rightarrow d$. The continuum eigenfunction χ_d is to be evaluated for the total molecular energy E_d. From the energy conservation we obtain $E_d = E_g + h\nu$, where E_g is the initial rovibrational energy of the molecule in the ground electronic state. In the dissociative state, the eigenfunctions have a maximum near the classical turning point and then, for larger *R* they become oscillating functions. Therefore the value of the integral (56) is largely determined by the behavior of eigenfunctions in the region of the inner turning point (provided that eigenfunction of the initial state is not be negligibly small in this region).

Our task was to calculate cross sections for the photodissociation of sodium molecule $Na_2(X^1\Sigma_g^+, v'')$ by λ_{PD} = 458 nm radiation from an Ar^+ ion laser for various possible initial vibrational levels v'' [publ7]. Such data were required for interpretation of an imaging experiment with the same photodissociation process.

Photodissociation cross sections are proportional to the square of transition matrix element between the initial and final molecular eigenstates. Our task is thus essentially reduced finding the vibrational eigenfunctions of the initial (bound) and final (dissociative) states.

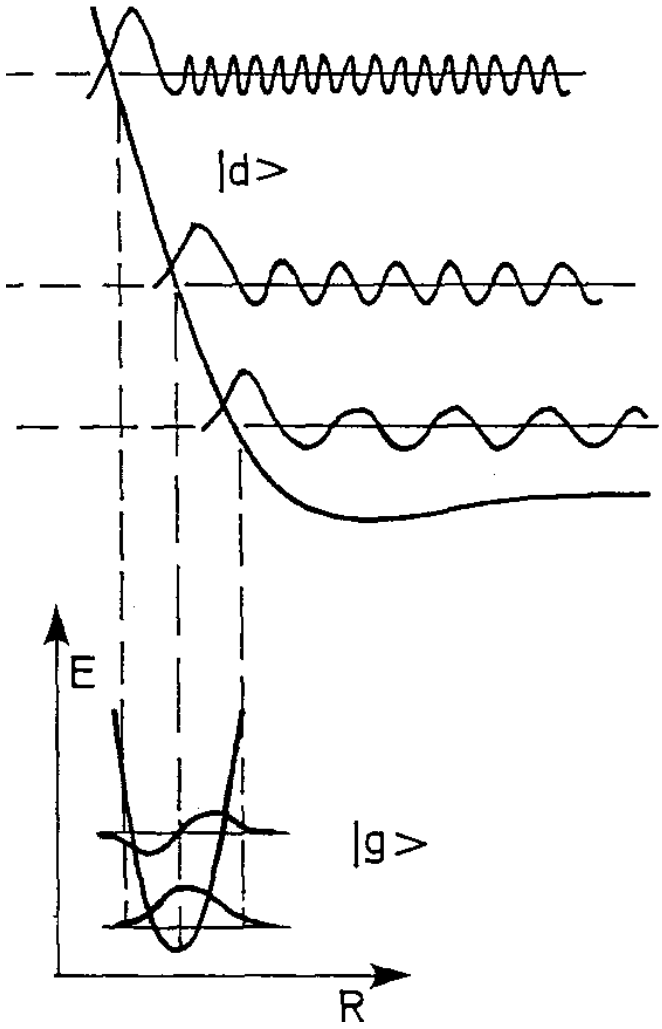

Fig. 13. Potential energy curves and wavefunctions for direct photodissociation. For the electronically excited state, eigenfunctions for continuum states at 3 different energies are shown. For the ground state, eigenfunctions of the two lowest vibrational levels are shown.

4.2. Experiment of $Na_2(X^1\Sigma_g^+)$ photodissociation process

Photodissociation of state selected sodium molecules, $Na_2(X^1\Sigma_g^+, v'') + h\nu \rightarrow Na_2^*(B^1\Pi_u) \rightarrow Na^*(3p_{3/2}) + Na(3s_{1/2})$ has been recently studied theoretically and experimentally at Kaiserslautern university using a novel "field-free" ion imaging

technique [publ7]. The experiment uses a supersonic Na/Na_2 beam in a combination with the stimulated Raman adiabatic passage (STIRAP) technique [73] to prepare Na_2 molecules in selected rovibronic levels of the electronic ground state $X^1\Sigma_g^+$. The molecules in levels $v'' \geq 10$ are photodissociated into $Na(3p_{3/2})$ and $Na(3s_{1/2})$ atomic fragments by the λ_{PD} = 458 nm radiation from an Ar^+ ion laser via the $B^1\Pi_u$ state. The excited $Na^*(3p_{3/2})$ photofragments were photoionized or excited to high Rydberg states (λ_{PI} = 408 nm) and registered by an ion imaging detector. The measured images showed not only the expected relatively fast photodissociation fragments, but also efficient formation of slow $Na(3p_{3/2})$ atoms. Fast and slow refer to the atomic velocity relative to the centre-of-mass of the dissociating molecule. Experimental ratio of the numbers of slow and fast photofragments is 0.16 and 0.22 for the dissociation of Na_2 from initial vibrational levels $v'' = 17$ and $v'' = 23$, respectively. Mechanism of the formation of slow $Na(3p_{3/2})$ atoms can be explained as consequence of radiation trapping on atomic resonance transitions. Fast $Na(3p_{3/2})$ atoms produced in the direct photodissociation process are surrounded by slow $Na(3s_{1/2})$ atoms in the ground state from the primary Na/Na_2 beam. Those slow $Na(3s_{1/2})$ atoms are excited to the $3p_{3/2}$ state via absorption of photons, which are emitted by the fast $Na(3p_{3/2})$ photofragments. Such mechanism is feasible, because the spontaneous lifetime of the $3p_{3/2}$ state is much shorter than the average time the photofragments need to escape from the primary particle beam. Most of the excited photofragments are therefore expected to emit a photon while surrounded by the $Na(3s_{1/2})$ atoms. This process could be well described in terms of the radiation trapping phenomenon.

4.3. Theory of $Na_2(X^1\Sigma_g^+)$ photodissociation process

In the calculation of $Na_2(X^1\Sigma_g^+, v''J'')$ photodissociation by the 458 nm photons of Ar^+ ion laser we assume that the fragmentation occurs exclusively via the $B^1\Pi_u$ state. The molecules are thus excited from a rovibronic level with energy $E(v''J'')$ in the electronic ground state into a dissociative state with energy $\varepsilon = E(v''J'') + h\nu_{Ar+}$ of the $B^1\Pi_u$ state. In the Born-Oppenheimer approximation, wavefunction of the initial and final molecular states can be separated into electronic and nuclear parts:

$$\left|\mathrm{X}^1\Sigma_g^+, \upsilon'' J'' M''\right\rangle = \left|\mathrm{X}^1\Sigma_g^+\right\rangle_{\mathrm{el}} \left|\mathrm{X}^1\Sigma_g^+, \upsilon'' J'' M''\right\rangle_{\mathrm{nuc}};$$

$$\left|\mathrm{B}^1\Pi_u^+, \varepsilon J' M'\right\rangle = \left|\mathrm{B}^1\Pi_u^+\right\rangle_{\mathrm{el}} \left|\mathrm{B}^1\Pi_u^+, \varepsilon J' M'\right\rangle_{\mathrm{nuc}},$$

where M is the projection of the nuclear angular momentum J onto the laboratory z-axis. The cross section of the photofragmentation depends on the frequency of the photodissociating photon and square of the transition moment [74, 75]. For linearly polarized light and isotropic distribution of the molecular axis in the initial state it can be written as:

$$\sigma\left(\mathrm{X}^1\Sigma_g^+, \mathrm{v}''\mathrm{J}'' \rightarrow B^1\Pi_u, \varepsilon \mathrm{J}'\right) = \frac{8\pi}{3c} \frac{\nu}{2\mathrm{J}''+1} \sum_{\mathrm{J}'=\mathrm{J}''-1}^{\mathrm{J}''+1} R^2_{\mathrm{X}^1\Sigma_g^+, \mathrm{v}''\mathrm{J}'' \rightarrow \mathrm{B}^1\Pi_u, \varepsilon \mathrm{J}'} \, \xi_{\mathrm{X}^1\Sigma_g^+, \mathrm{J}'' \rightarrow \mathrm{B}^1\Pi_u, \mathrm{J}'}$$

Here, c is the speed of light, where $\xi_{\mathrm{X}^1\Sigma_g^+, \mathrm{J}'' \rightarrow \mathrm{B}^1\Pi_u, \mathrm{J}'}$ is the sum of squares of the angular part of transition moment over the magnetic quantum numbers M [76, 77] described by 3-j-symbol:

$$\xi_{\mathrm{X}^1\Sigma_g^+, \mathrm{J}'' \rightarrow \mathrm{B}^1\Pi_u, \mathrm{J}'} = \sum_{M=-\mathrm{J}}^{+\mathrm{J}} \left|R^{rot}_{\mathrm{J}''\mathrm{J}'}\right|^2 = \frac{1}{3}(2\mathrm{J}''+1)(2\mathrm{J}'+1) \begin{pmatrix} \mathrm{J}'' & 1 & \mathrm{J}' \\ 0 & 1 & -1 \end{pmatrix}^2$$

This expression takes into account that for lineary plolarized light ΔM=0. The radial part of the matrix element can be written as:

$$R_{\mathrm{X}^1\Sigma_g^+, \mathrm{v}''\mathrm{J}'' \rightarrow \mathrm{B}^1\Pi_u, \varepsilon \mathrm{J}'} = \int \chi_{\mathrm{X}^1\Sigma_g^+, \mathrm{v}''\mathrm{J}''}(R)\, \mu(R)\, \chi_{B^1\Pi_u, \varepsilon \mathrm{J}'}(R) dR. \qquad (57)$$

The values for the transition dipole moments $\mu = e\left\langle \mathrm{X}^1\Sigma_g^+ \left| \sum q_i \right| \mathrm{B}^1\Pi_u \right\rangle_{\mathrm{el}}$ (where e is the electron charge and q_i are the electronic coordinates) and the potential curves were taken from [12]. The authors of [12] used the combined valence configuration interaction and the core polarization potential method to obtain potential curves and electronic dipole moment functions μ as a function of internuclear distance R. In this study, the radial wavefunctions $\chi_{\mathrm{X}^1\Sigma_g^+, \mathrm{v}''\mathrm{J}''}(R)$ and $\chi_{B^1\Pi_u, \varepsilon \mathrm{J}'}(R)$ in eq. (57) were integrated numerically using the Numerov method [53]. The resulting photodissociation cross sections for the vibrational level range of interest are given in fig. 14. In the calculations we have also checked for possible contribution of the fragmentation of molecules into $Na(3p_{1/2})$ and $Na(3s_{1/2})$ atoms via the $A^1\Sigma_u^+$ state. These calculations showed that for the 458.06 nm photons this fragmentation channel is by several orders of magnitude less efficient than

the fragmentation via the $B^1\Pi_u$ electronic state and can be safely considered as negligible. Note, that besides the $A^1\Sigma_u^+$ and $B^1\Pi_u$ states there are no other singlet ungerade states in the considered energy range, so that the $B^1\Pi_u$ state is the sole dissociation gateway.

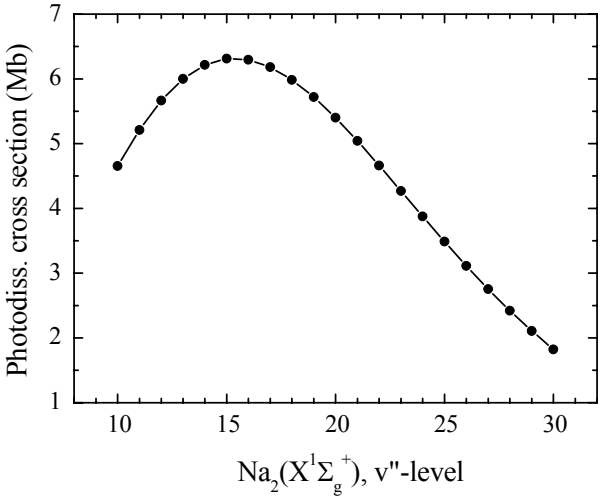

Fig. 14. Cross sections for photofragmentation of Na_2 ($X^1\Sigma_g^+$, v", J"=9) molecules by 458 nm photons via the $B^1\Pi_u$ state. For levels $v" \leq 9$ the energy $\varepsilon = E(v"J") + h\nu_{Ar+}$ is not sufficient to overcome the potential barrier of the $B^1\Pi_u$ state, the maximum of which lies 46 meV above the $3p_{3/2} + 3s_{1/2}$ dissociation asymptote [78]. In the experiment, no detectable photofragment signals were registered for photodissociation from the v"=9, J"=9 level.

4.4. Conclusion

In this thesis work [publ7] we have performed theoretical studies of the photodissociation process $Na_2(X^1\Sigma_g^+, v",J") + h\nu_{458nm} \rightarrow Na_2^*(B^1\Pi_u) \rightarrow Na^*(3p) + Na(3s)$ within the framework of Born-Oppenheimer approximation. The energy balance showed that for levels $v" \leq 9$ the energy of photon with wavelength 458 nm is not sufficient to overcome the potential barrier of the $B^1\Pi_u$ state. Therefore, the photodissociation cross sections were calculated beginning from the v"=9, J"=9 level up to v"=30. We proved that $Na_2(X^1\Sigma_g^+)$ photodissociation with 458 nm photons can proceed only via the $B^1\Pi_u$ state. In our calculations, we used more realistic transition dipole moment $\mu(R)$, which depends on the internuclear distance R. Such approach yields more accurate results than those obtained using the Franc-Condon approximation, which is frequently involved due to its simplicity.

5. Summary

According to the tasks set for the present promotion work, the following results were obtained:

- Investigation of stochastic phenomena occurring during the passage of the colliding $A^{**} + A$ complex through the zone of multiple overlapping level crossings [publ1, publ3, publ4] were caried out. Based of this investigation, an essential improvement of the DSMJ model (Duman-Shmatov-Mihajlov-Janev) was achieved, which includes the stochastic description of Rydberg electron motion during the collision [publ3]. In addition, effects of collisional *l*-mixing, twisting effect, and blackbody radiation (BBR) and spontaneous decay induced mixing of Rydberg states were taken into account. Our theoretical results were compared with the associative ionization rate constants of crossed-beam experiments with sodium atoms in *n*P states with *n*=5–15 [34] and single-beam experiments with Na atoms in *n*S, *n*P, *n*D states [19, 35, publ2]. We used our developed approach to calculate the associative ionization rate constants in Na^{**} + Na collisions, and it was shown that the stochastic model yields a substantially better agreement with the experimental data than the DSMJ model, which was formerly traditionally used for the analysis of ionization processes of type (1) [publ3].
- General analytical approach was developed for the solution of Biberman-Holstein radiation trapping equation [10, 67, publ6]. Our geometric quantization technique (GQT) introduces a quasi-particle and uses quantization rules in order to solve Biberman-Holstein radiation trapping equation in form of a wave equation. In this thesis we extended our method to 3-dimensional vapour cells. In the first step, we have computed the phase shift that a quasi-particle suffers upon reflection from the cell surface by a certain angle θ. The angles of incidence of the incoming rays (quasi-particles) vary with the position on the cell surface. Because of this variation the averaged phase shift was introduced (52). We calculated radiation trapping factors g_0 for complicated geometries of vapour cells, including elliptical cylinders, prolate and oblate ellipsoids. A comparision the results of much more demanding numerical

Monte-Carlo calculations showed that the accuracy of our calculations is about 5%. The GQT technique enables the solution of a large range of practical problems of radiation trapping with very little numerical effort. It is more general than other available analytical methods. In this thesis we give a simple and ready-to-use recipe for the computation of trapping factors in plane-parallel slabs, finite cylinders, spheres, and elliptical cells.

- Model potential method was used to obtain Na $3p_{3/2} \leftarrow (ns_{1/2}, nd_{5/2,} nd_{3/2})$ transition probabilities for Rydberg states with $n \leq 50$ and photoionization cross sections of Na($3p_{3/2}$) atoms to the continuum [publ5]. Wave functions were calculated numerically by solving the Schrodinger equation for the valence electron of Na atom. For this purpose, the potential for Na valence electron was derived as. Coulomb potential of the unperturbed Na^+ ion (Eq. (31)). The core polarization effect was also taken into account. Core polarization affects the calculations of transition matrix elements in the way that it changes the wave functions and the dipole transition operator. In our calculations we used the exchange potential and the parametric core polarization potentials of Na given by Weisheit [40] and Meyer [55]. Tests with various parameter sets of those potentials allowed us to estimate the accuracy of our method. Lifetimes, transition probabilities, and photoionization cross sections obtained in this thesis were compared with the available experimental data and with other theoretical calculations. We believe that model potential method with parametric core polarization potential can be made quantitatively reliable if one or more parameters of this parametric potential, are chosen as empirical parameters by fitting them to the experimental binding energies of the valence electron. The estimated accuracy of our results is better than 5%. The dipole transition moments for the discrete states and the continuum are also presented in a form of analytical expression.
- Theoretical study of the photodissociation process $Na_2(X^1\Sigma_g^+, v'',J'') + h\nu_{458nm} \rightarrow Na_2^*(B^1\Pi_u) \rightarrow Na^*(3p) + Na(3s)$ within the framework of the Born-Oppenheimer approximation was performed [publ7]. In this study, the Na_2 molecules are excited from a rovibronic level (v'',J'') in the electronic ground state $X^1\Sigma_g^+$ to the dissociation continuum of the $B^1\Pi_u$ state by polarized light with wavelength λ_{PD}=458 nm from an

Ar^+ ion laser. The radial wave functions of the vibronic states of the electronic ground state $X^1\Sigma_g^+$ and continuum wave functions of the final state $B^1\Pi_u$ were calculated numerically by solving the Schrodinger equation. The photodissociation cross sections were calculated as a function of the initial ground state vibrational level υ". We showed that $Na_2(X^1\Sigma_g^+)$ photodissociation by 458 nm photons can proceed only via the $B^1\Pi_u$ state, while the fragmentation via the $A^1\Sigma_u^+$ state can be considered as negligible.

References:

[1] T. B. Lucatorto and T. J. McIlrath, Appl. Opt. 19, 3948 (1980).

[2] A. Dalgarno and J. H. Black, Rep. Prog. Phys. 39, 573 (1976).

[3] J. Weiner, F. Masnou-Seeuws, and A. Giusti-Suzor, Adv. At. Mol. Opt. Phys. 26, 209 (1990).

[4] A. N. Klucharev and V. Vujnović, Phys. Reports 185, 55 (1990).

[5] D. Mihalas, Stellar Atmospheres (Freeman, San Francisco, 1978), 2nd ed..

[6] A. F. Molisch and B. P. Oehry, Radiation Trapping in Atomic Vapours (Oxford University, Oxford, 1998).

[7] M. N. Berberan-Santos, E. Pereira, and J. M. G. Martinho, in Resonance Energy Transfer,edited by D. L. Andrews and A. A. Demidov (John Wiley & Sons, Chichester, 1999).

[8] F. Bardou, J. P. Bouchaud, A. Aspect, and C. Cohen-Tannoudji, Levy Statistics and Laser Cooling (Cambridge University, Cambridge, England, 2002).

[9] T. Holstein, Phys. Rev. 72, 1212 (1947).

[10] N. N. Bezuglov, Molisch A., Klucharev A.N., Fuso F., Allegrini M.// Phys. Rev. A 59, 4340 (1999).

[11] Kaufmann O, Ekers A, Gebauer-Rochholz C, Mettendorf K U, Keil M and Bergmann K 2001 Int. J. Mass. Spectrom. 205 233

[12] I. Schmidt, Diplomarbeit (Universität Kaiserslautern, Kaiserslautern 1987). The potentials are also available upon request from W. Meyer.

[13] Weiner J, Bagnato V S, Zilio S, Julienne P S, 1999 *Rev. Mod. Phys.* 71 1.

[14] Gallagher T F 1994 Rydberg Atoms (Cambridge: Cambridge University Press)

[15] A.N., Klyucharev *Usp. Fiz. Nauk*, 163, 39 (1993).

[16] Duman E L and Shmatov I P 1980 *Sov. Phys. JETP* 51 1061

[17] R.K.Janev and A.A.Mihajlov, Phys. Rev. A, 21, 819 (1980).

[18] A.A.Mihailov and R.K.Janev, J. Phys. B, 14, 1639 (1981).

[19] J.Weiner, J.Boulmer, J. Phys. B, 19, 599 (1986).

[20] N.N.Bezuglov, V.M.Borodin, A. K. Kazanskii, A.N.Klyucharev, A.A.Matveev, and K.V.Orlovskii, Opt. Spectrosc. 91, 25 (2001).

[21] Nikitin E E and Umansky S Y 1984 Theory of Slow Atomic Collisions (Springer. New York)
[22] N.N.Bezuglov, V.M.Borodin, A.Ekers and A.N.Klyucharev, Opt. Spectrosc., 93, 721 (2002)
[23] Beigman I.L., Lebedev V.S. Physics Reports, 250, 95 (1995).
[24] Nikitin E. and Smirnov B. Sov. Phys. Usp., 21, 95 (1978)
[25] Nikitin E E and Umansky S Ya 1984 *Theory of Slow Atomic Collisions* (New York: Springer)
[26] N.N.Bezuglov, V.M.Borodin, A.N.Klucharev, F.Fuso, M.Allegrini, K.V.Orlovsky and M.L.Janson, Opt. Spektrosc. 86, 824 (1999).
[27] Zaslavsky M.G. Physics of Chaos in Hamiltonian systems. (Imperial College Press, River Edge, N.J., 1998).
[28] Reichl L.E. The Transition to Chaos In Conservative Classical Systems: Quantum manifestations (Springer-Verlag New York, 1992).
[29] Jensen R.V., Sussckind S.M., and Sanders M.M. Phys.Rep. 1991,..201., P.1.
[30] Matrasulov D.U. Phys. Rev. A, 60 , 700 (1999).
[31] Delone N.B., Zon V.A., and Krainov V.P., Sov. Phys. JETP, 48, 223 (1978).
[32] Gontis V., and Kaulakys B., J.Phys.B. 1987.20. P.5051.
[33] N.N.Bezuglov, V.M.Borodin, Opt. and Spectrosc., 86, 467 (1999).
[34] J.Boulmer, R.Bonanno, J.Weiner, J. Phys. B, 16, 3015 (1983).
[35] S.B.Zagrebin, A.V.Samson, J. Phys. B, 18, L217 (1985).
[36] Nesmeyanov A N Vapour pressure of the chemical elements (Elsevier, Amsterdam / London / New York, 1963)
[37] Browning P and Potter P E An Assessment of the Experimentally Determined Vapour Pressures of the Liquid Alkali Metals, Chapter 6.2 in Handbook of Thermodynamic and Transport Properties of Alkali Metals (IUPAC, Blackwell Scientific Publications, Boston, 1985)
[38] D.R. Bates, A. Damgaard, Philos. Trans. R. Soc. London, Sect. A 242, 101 (1949).
[39] A.Lingaard, S.E. Nielsen, Data Nucl. Data Tables 19, 533 (1977).
[40] J.W. Weisheit, Phys. Rev. A. 5, 1621 (1972).
[41] D.W. Norcross, Phys. Rev. A. 7, 606 (1973).

[42] C. Laughlin, J. Phys. B 11, 1399 (1978).

[43] H.T. Duong, J. Pinard, J.L. Vialle, J. Phys. B 11, 797 (1978).

[44] C.E. Theodosiou, Phys. Rev. A 30, 2881 (1984).

[45] C. Laughlin, Phys. Scr. 45, 238 (1992).

[46] Davydkin, V. A. and Zon, B. A., Opt. Spektr., 1982. vol. 52, no. 2, p. 386.

[47] Bureeva, L. A., Astron. Zh., 1968, vol. 45, p. 1218

[48] Aymar M.,Robaux O.,Wane S.//J.Phys.B.1984.V.17. P.993.

[49] C. Guet, S. A. Blundell, and W. R. Johnson, Phys. Rev. A 49, 2181 (1994).

[50] S. Salomonson and A. Ynnerman, Phys. Rev. A 43, 88 (1991).

[51] T. Brage, C. Froese Fischer, P. Jönsson, Phys. Lett. A 143, 384 (1990).

[52] P. Jönsson, A. Ynnerman, C. Froese Fischer, M. R. Godefroid, and J. Olsen Phys. Rev. A 53, 4021 (1996).

[53] B.R.Johnson, JCP 67, 4086 (1977).

[54] C. Bottcher, J. Phys. B 4, 1140 (1971).

[55] W. Müller, J. Flesch,W. Meyer J. Chem. Phys. vol. 80, No 7, 3311 (1984).

[56] I.D. Petrov, V.L. Sukhorukov, H. Hotop, J. Phys. B 32, 973 (1999).

[57] W.C. Martin, R. Zalubas, J. Phys. Chem. Ref. Data 10, 153 (1981).

[58] Sobelman, I.I., Vvedenie v teoriyu atomnyh spektrov (Introduction to the Theory of Atomic Spectra), Moscow: Nauka, (1977).

[59] S. Hameed, A. Herzenberg, and M. G. James, J. Phys. B 1, 822 (1968).

[60] D.E.J. Rothe, J. Quant. Spectrosc. Radiat. Transfer 9, 49 (1969).

[61] C.E. Burkhardt, J.L. Libbert, Xu. Jian, J.J. Leventhal, J.D. Kelley, Phys. Rev. A 38, 5949 (1988).

[62] J.M. Preses, C.E. Burkhardt, R.L. Corey, D.L. Earsom, T.L. Daulton, W.P. Garver, J.J. Leventhal, A.Z. Msezane, S.T. Manson, Phys. Rev. A 32, 1264 (1985).

[63] I.D. Petrov, V.L. Sukhorukov, E. Leber, H. Hotop, Eur. Phys. J. D 10, 53 (2000).

[64] M. Aymar, E. Luc-Koenig, F. Combet Farnoux, J. Phys. B 9, 1279 (1976).

[65] A. G. Mitchell and M. W. Zemanski, Resonace Radiation And excited atoms (Cambridge Univ. Press, Cambridge, 1961)

[66] Нагирнер Д. И. Перенос излучения в линиях молекул и атомов. Препринт Ин-та космических исследований № 457. М., 1979. 24 с. 25.

[67] Bezuglov N.N., Molisch A., Klucharev A.N., Fuso F., Allegrini M.// Phys. Rev. A, 57, 2612 (1998)

[68] Перель В. И., Рогова И. В. Релаксация распределения возбужденных атомов по скоростям и поляризации при полном пленении резонансного излучения – Журнал эксп. и теор. физ. 1971. Т. 61. С. 1815-1821. 26.

[69] A. Corney, Atomic and Laser Spektroscopy (Oxford University Press, Oxford, 1977).

[70] V. V. Ivanov, Transfer of Radiation in Spectral lines, Natl. Bur. Stand. (U.S.) Special Publ. No. 385 (U.S. GPO, Washington, D.C., 1973).

[71] L. D. Landau and E. M. Lifshitz, *Quantum Mecahnics* (Pergamon, Oxford, 1965).

[72] G. Herzberg, Molecular spectra and Molecule structure, vol. 1 and 3, Van Nostrand, New-York (1950)

[73] K. Bergmann, H. Theuer, and B. W. Shore, Rev. Mod. Phys. 70, 1003 (1998); U. Gaubatz, P. Rudecki, S. Schiemann, and K. Bergmann, J. Chem. Phys. 92, 5363 (1990).

[74] J.-A. Beswick and J. Durup, in *Half Collisions Induced by Lasers*, Proceedings of the Summer School on Chemical Physics, Les Houches, France, edited by P. Glorieux, D. Lecler, and R. Vetter (Ed. CNRS, Paris, 1979).

[75] A. Messiah, *Quantum Mechanics* (North Holland, Amsterdam, 1962) Vol. 2.

[76] I. Kovacs, *Rotational Structure in the Spectra of Diatomic Molecules* (Adam Hilger LTD, Lodon, 1969).

[77] B. R. Judd, *Angular Momentum Theory for Diatomic Molecules* (Academic, New York, 1975).

[78] E. Tiemann, Z. Phys. D 5, 77 (1987).

[79] P. M. Koch and K. A. Leeuwen, Phys. Rep. 225, 289 (1995).

[80] L. D. Landau and E. M. Lifshitz, Course of Theoretical Physics, Vol. 2: The Classical Theory of Fields, 7nd ed. (Nauka, Moscow, 1988).

The results obtained have also been reported at several conferences:

1. **K. Miculis**, W. Meyer, "*Transition propabilities from Na(3p3/2) to discrete and continuum states*", in: Abstracts of the 7th European Conference on Atomic and Molecular Physics, ECAMP VII, Berlin, Germany, edited by H. Rottke, U. Eichmann, and W. Sander (EPS, Berlin, 2001)

2. N. Bezuglov, V. M. Borodin, A. N. Klucharev, A. Ekers, and **K. Miculis**, *"Quasiclassical description of chaotic dynamics in Rydberg atom collisions"*, in: Abstracts of the 34th EGAS Conference, Sofia, Bulgaria, edited by K. Blagoev (EPS, Sofia, 2002), Europhysics Conference Abstracts Vol. 26C, pp. 92-93.

3. A. Ekers, O. Kaufmann, K. Bergmann, **K. Miculis**, M. Auzinsh, N. Bezuglov, and W. Meyer, *"Field-free imaging of photofragmentation of Na_2"*, in: Abstracts of the 34th EGAS Conference, Sofia, Bulgaria, edited by K. Blagoev (EPS, Sofia, 2002), Europhysics Conference Abstracts Vol. 26C, pp. 78-79.

4. **K. Miculis**, N. N. Bezuglov, A. K. Kazansky, A. N. Klucharev, **A. Ekers**, F. Fuso, M. Allegrini, *Semiclassical treatment of radiation imprisonment in spatially nonuniform vapour*, in: Abstracts of the XXIII ICPEAC (Stockholm, 2003), p. Mo034.

5. **K.Miculis**, I.I.Beterov, N.N.Bezuglov, A.Ekers, I.I.Ryabtsev, D.B.Tretyakov, and A.N.Klucharev, *Stochastic dynamics in the Associative Ionization of Rydberg atoms,* in: Abstracts of the 37th EGAS (Dublin 2005), p1:32, 119

ACKNOWLEDGEMENTS

Thanks are due to prof. Nikolay Bezuglov (Николай Безуглов) and prof. Viachaslav Borodin (Вятчеслав Бородин). In collaboration with prof. Nikolay Bezuglov from St. Petersburg State University a significant part of my promotion work was carried out. I express gratitude also to my supervisor, prof. Marcis Auzinsh, and members of our research group Konstantin Orlovsky, who helped me with advices about numerical calculations and programming, and Vladimir Grushevsky for support in theory, and whom I value very highly as a colleague. Thanks are due to Dr. Aigars Ekers, who supported me by research in Kaiserslautern university. I would also like to thank prof. Klaas Bergmann and his workgroup from the University of Kaiserslautern. I acknowledge prof. Wilfried Meyer, with whom I have had a pleasure to work or to discuss with.